Linking proximal ignimbrites and coeval distal tephra deposits to establish a record of voluminous Early Quaternary (2.4-1.9 Ma) volcanism of the Tauranga Volcanic Centre, New Zealand

Marlena Prentice[a*], Adrian Pittari[a], David J. Lowe[a], Geoff Kilgour[b], Peter J.J. Kamp[a], Miriam Namaliu[a]

[a]*School of Science-Te Aka Mātuatua, University of Waikato, Hamilton, New Zealand*

[b]*GNS Science, Wairakei*

*Corresponding author

Email: prenticelm@gmail.com

Abstract

The Tauranga Volcanic Centre (TgaVC) of the North Island, New Zealand, was active from 2.95 to 1.9 Ma. It lies temporally and spatially between the currently active Taupō Volcanic Zone, one of the most productive regions of Quaternary silicic volcanism globally, and its predecessor, the Coromandel Volcanic Zone. This study provides an enhanced chronology for pyroclastic volcanism of the TgaVC with four locally widespread units named and defined as follows: Welcome Bay and Wharo ignimbrites (together formerly known as Lower Pāpāmoa Ignimbrite); Otawera Ignimbrite; and Arateka Ignimbrite (formerly known as Upper Pāpāmoa Ignimbrite). These eruptives were followed by the eruption of the large-volume Waiteariki Ignimbrite at 2.1 Ma. In northern Hawke's Bay (150-170 km southeast of TgaVC), several distal tephra-fall horizons and an ignimbrite (Hikuroa Pumice Member) are preserved in marine-hosted sediments and are stratigraphically equivalent to the five ignimbrites of the TgaVC. Using new major- and trace-element data on glass in conjunction with new zircon-derived U-Pb ages, a correlation between the Hawke's Bay tephras and the TgaVC ignimbrites is established and the Hikuroa Pumice Member is confirmed as the distal deposit of the Waiteariki Ignimbrite. The integrated proximal and distal records show that at least eight eruptions occurred in the TgaVC between 2.4 and 1.9 Ma and provide a maximum repose period between explosive eruptions of ca. 50 kyrs.

Keywords

Taupō Volcanic Zone; Coromandel Volcanic Zone; Tauranga Volcanic Centre; Tephrochronology; U-Pb zircon geochronology; Geochemistry

1. Introduction

Sequences of tephra deposits produced by explosive volcanic activity play an important role in helping to construct the eruptive histories of large silicic volcanic fields. In proximal regions, the record of volcanism is often incomplete due to burial or destruction by subsequent volcanic activity and/or, tectonism and by the preferential erosion of unconsolidated pyroclastic deposits rather than resistant welded ignimbrites and lavas. In contrast, medial to distal tephra archives found within lacustrine, marine and ice-cores can provide more detailed records of mainly rhyolitic volcanism which, when combined with proximal records, provide valuable information about eruptive histories of long-lived silicic systems (Carter *et al.*, 2004; Kutterolf *et al.*, 2016; Lukács *et al.*, 2018; Amma-Miyasaka *et al.*, 2020). The use of tephrostratigraphy underpins such records and, together with stratigraphic superpositioning, is focused on the mineralogical and geochemical correlation and dating of key tephra units (Lowe, 2011).

The correlation of widespread distal tephras to proximal deposits originating from single eruption episodes provides an understanding of the eruptive histories, eruption volumes and recurrence intervals (Ponomareva *et al.*, 2015) and provide robust intra- and inter-regional isochronous marker beds which can then be used within a wide range of fields (Hopkins *et al.*, 2021a). These correlations then form the basis to determine distributions to reliably estimate and/or re-evaluate eruptive volumes and magnitudes of significant volcanic events (Kutterolf *et al.*, 2016; Ponomareva *et al.*, 2018; Silleni *et al.*, 2021). Additionally, geochemical analysis of the tephras (primarily glass shard constituents) can led to identification of source volcanoes (Kutterolf *et al.*, 2016) and magmatic evolution (Bryant *et al.*, 2003; Straub *et al.*, 2015; Pearce *et al.*, 2020).

Within the North Island of New Zealand, the modern loci of arc-related volcanism occurs within the Taupō Volcanic Zone (TVZ) **(Fig.1)**. Active for c. 2 Myr, the TVZ has a long and complex history, yet it is only the latest manifestation of volcanism in New Zealand. Prior to activity within the TVZ, rhyolitic volcanism migrated southeast through the Coromandel Volcanic Zone (CVZ; 12-3.5 Ma). Combined, the CVZ and TVZ have created an extensive rhyolitic tephra record dating back over 12 Myr (Carter *et al.*, 2004). Yet despite this comprehensive record, very few correlations have been established between tephra-fall deposits and known proximal deposits because the chronological and geochemical record defining the history of volcanism in many source locations and their products remains poorly defined (Hopkins *et al.*, 2021b).

The silicic Tauranga Volcanic Centre (TgaVC), located in the Bay of Plenty region of North Island, New Zealand **(Fig. 1)**, was active from 2.95 to 1.90 Ma (Pittari *et al.*, 2021). Volcanism of the TgaVC lies temporally and spatially between the defined locations and time frames of activity in TVZ and CVZ.

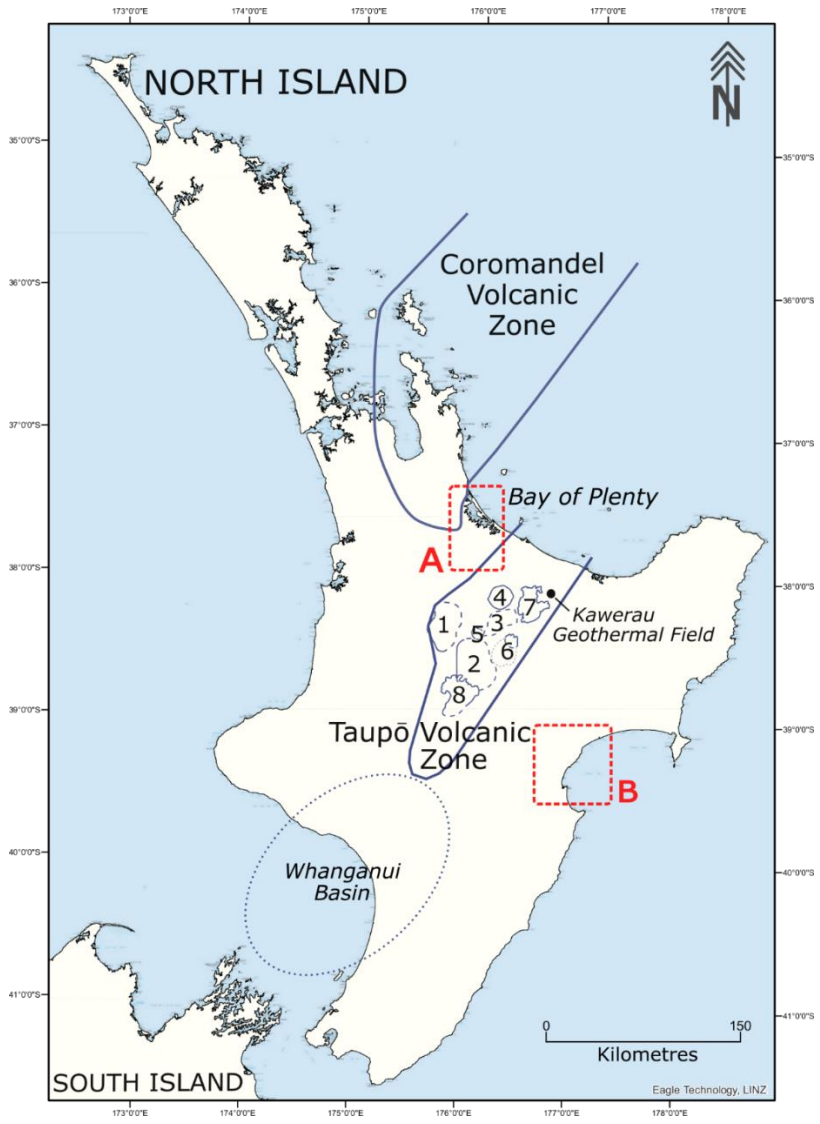

Figure 1. Map showing main centres of rhyolitic volcanism active in North Island since c. 3 Ma: the Coromandel Volcanic Zone (CVZ) (active c. 12–3.5 Ma (Carter *et al.*, 2004; Pittari *et al.*, 2021) and Taupō Volcanic Zone (TVZ) (active since c. 2 Ma) (Wilson & Rowland, 2016), and the locations of the Whanganui Basin and Bay of Plenty (A) and Hawke's Bay (B) regions depicted in Figure 2. Numbered TVZ calderas are numbered as follows: 1, Mangakino; 2, Whakamaru; 3, Kapenga; 4, Rotorua; 5, Ohakuri; 6, Reporoa; 7, Okataina; 8, Taupō (after Leonard et al., 2010).

Despite its importance as a key transition centre between these two broader volcanic zones, understanding of volcanism during this period remains limited (Briggs *et al.*, 2005; Pittari *et al.*, 2021). This study provides an enhanced chronology for volcanism of the TgaVC and we undertake new analyses of both ignimbrites in the TgaVC and stratigraphically-equivalent tephra horizons in northern Hawke's Bay which is located 150-170 km southeast of Tauranga **(Fig. 1)**. Using major- and trace-element analyses of glass in conjunction with new zircon-derived U-Pb ages, we examine and test the

previous assumption that tephra deposits preserved within northern Hawkes' Bay marine sediments (2.4–1.63 Ma) were sourced from a vent region located in the TgaVC, primarily due to the similar ages of proximal deposits in the Tauranga region **(Fig. 2a)** (Hopkins and Seward, 2019). These correlatives are linked in turn to other previously identified horizons, both onshore and offshore. The main focus of this paper is to demonstrate the multi-faceted approach required to confidently correlate proximal and distal pyroclastic deposits from the Early Quaternary period in order to establish a comprehensive eruptive history for the TgaVC. The petrogenesis of the magmas is not investigated here, but will be presented in subsequent papers. We follow the definition in Lowe (2011) where the term "tephra" (*sensu lato*) refers to all unconsolidated pyroclastic products of volcanic eruptions including both fall deposits and those arising from (non-welded) pyroclastic density currents (pyroclastic flows or surges). For additional clarity, specific pyroclastic deposits are referred to as either tephra-fall, or distal or proximal ignimbrites.

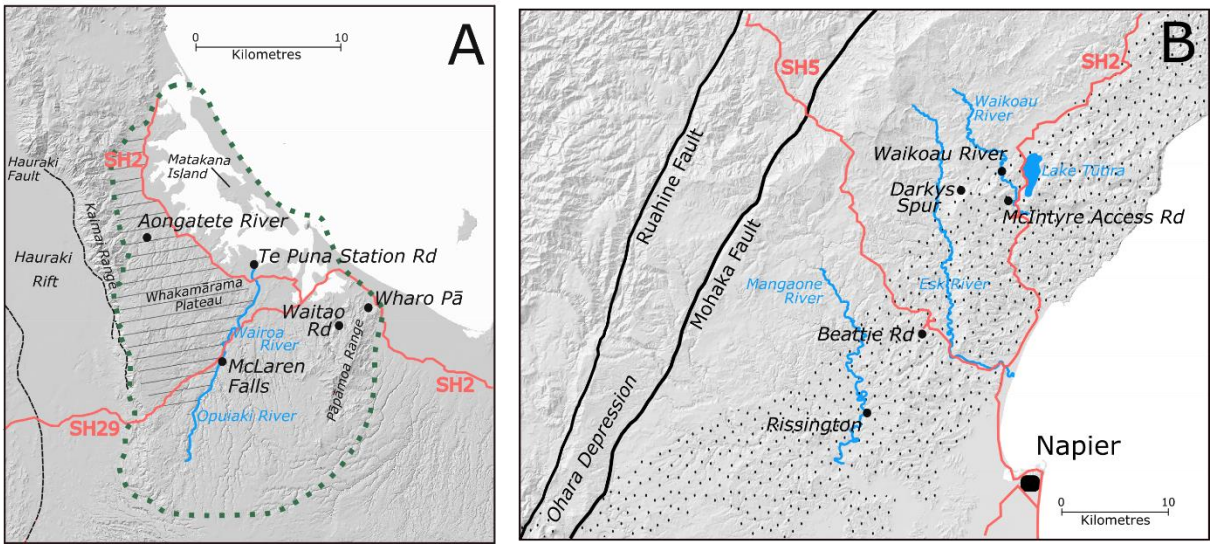

Figure 2. (A) Tauranga region with sample locations and features mentioned in the text with the extent of the Tauranga Volcanic Centre outlined in green dots. **(B)** Northern Hawke's Bay with sample location sites and names referred to in the text. The Ruahine and Mohaka faults are the two major dextral strike-slip faults in central parts of the North Island Fault system, which bound the Ohara Depression. Stippled area shows regional extent of 2.4–1.63 Ma marine sedimentary deposits (known as the Esk and Petane formations) in which distal tephras have been preserved. State highways (SH) in red.

2. TgaVC pyroclastic stratigraphy and tephrostratigraphy of northern Hawke's Bay

2.1 Tauranga Volcanic Centre

Deposits of the TgaVC **(Fig. 2a)** consist of an eroded andesitic stratovolcano (Otawa Formation), numerous rhyolite-dacite lava dome or dome complexes (Minden Rhyolite Subgroup), a single emergent exposure of basalt found off the coast of Matakana Island within the Tauranga Harbour, and several ignimbrites within the Waitearikiand Pāpāmoa formations. Although the source(s) of these ignimbrites is yet to be formally defined, they are inferred to be of local (i.e. TgaVC) origin (Briggs *et al.*, 2005; Pittari *et al.*, 2021). Radiometric age determinations of deposits of the TgaVC have been undertaken using K-Ar (Takagi, 1995), $^{40}Ar/^{39}Ar$ (Briggs *et al.*, 2005), and U-Pb and (U-Th)/He (Pittari *et al.*, 2021) methods on whole-rock and crystal separates. Together, these dates have provided understanding of the volcanic stratigraphy of major geological units **(Fig. 3)** within the region and insight into the evolution of the TgaVC. Prominent ignimbrite units selected for analysis in this study are described below.

2.1.1 Waitearikiignimbrite

The welded Waitearikiignimbrite is the most prominent and voluminous pyroclastic unit of the TgaVC. It is exposed throughout the eastern foothills of the Kaimai Range and underlies the gently sloping upper surface of the Whakamārama Plateau **(Fig. 2a)** (Houghton & Cuthbertson, 1989; Briggs *et al.*, 1996). Exposures are also found along the western margin of the Pāpāmoa Range. Throughout central and southern areas, the Waitearikiignimbrite is buried by younger TVZ-derived deposits where it is encountered in drill holes at a depth of 50–150 m with thicknesses exceeding 200 m in some localities (Houghton & Cuthbertson, 1989; Briggs *et al.*, 1996). This ignimbrite unit is a crystal- and pumice-rich, lithic-poor ignimbrite which is extensively welded and has pronounced eutaxitic texture **(Fig. 4a)**. The predominant mineral assemblage comprises is plagioclase, hornblende, pyroxene, and quartz with minor amounts of biotite with rare lithic clasts (<2 %), predominantly derived from rhyolite lava (Briggs *et al.*, 1996). In outcrop, the Waitearikiignimbrite is pervasively devitrified making the groundmass glass unsuitable for geochemical analysis. However, during the 1970s, a series of cores were drilled across the eastern side of the southern Kaimai Range as part of geological investigations for the Kaimai Rail Tunnel (Healy, 1967; Hegan, 1972). Located near the eastern portal above the Aongatete River **(Fig. 2a)**, one such core, ES112, intersected 157 m of Waitearikiignimbrite with light-brown perlitic glass preserved in the lower 10 m, a phenomenon documented in some other highly welded ignimbrites (e.g. Fish Canyon Tuff; Bachmann *et al.* 2002), and this basal glass provided material for geochemical analysis (see **Section 5.1.2** for discussion).

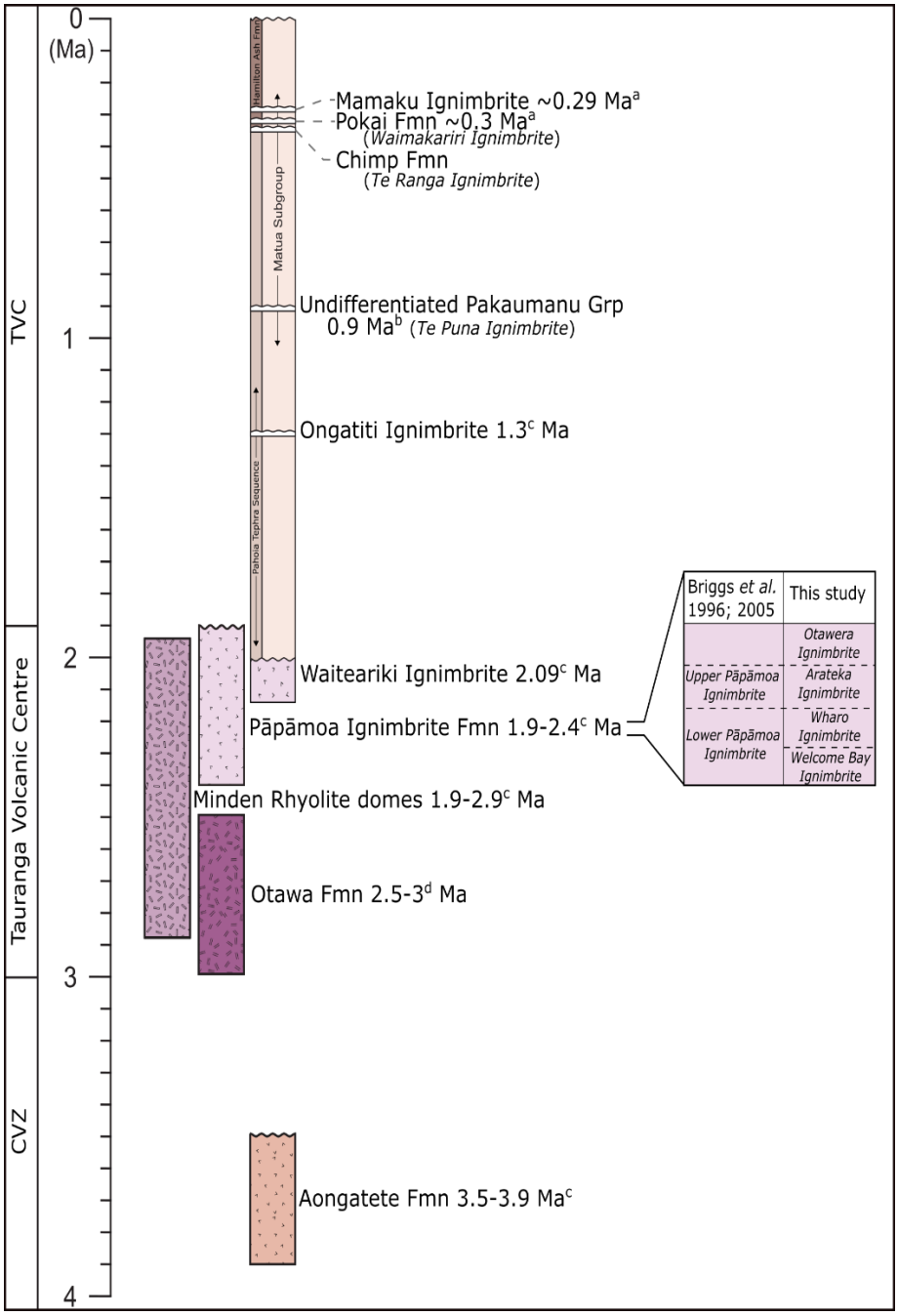

Figure 3. Generalised stratigraphy of the Tauranga region including deposits associated with TgaVC. Italicised names in parentheses, represent ignimbrites defined by Briggs *et al.* (1996). Ages obtained from Downs *et al.* (2014)[a]; Briggs *et al.* (2005)[b]; Pittari *et al.* (2021)[c]; Stipp (1968)[d]. Fmn, Formation; Grp, Group. Note that in this study we refer to four newly-named ignimbrite units within the Pāpāmoa Formation, amended from Briggs *et al.* (1996; 2005). See text for details.

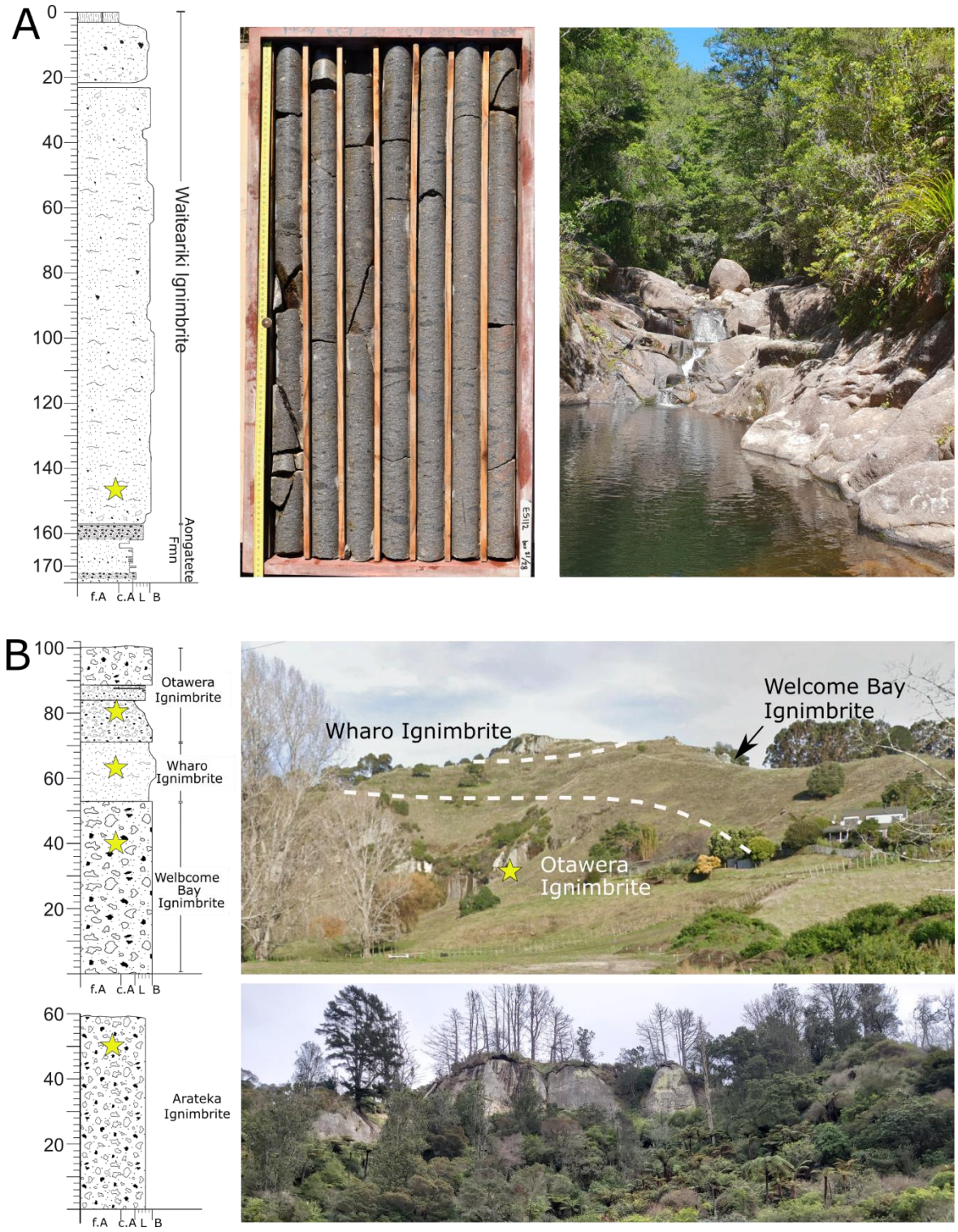

Figure 4. Simplified stratigraphic log and a photograph of pyroclastic deposits of the TgaVC. **(A)** Section of core ES112 through the Waitearikí Ignimbrite (left; see text); photo (right) shows a typical outcrop for the Waitearikí Ignimbrite (Aongatete River). **(B)** Outcrop photographs demonstrating the stratigraphic relationships of the newly named ignimbrite unit of the Pāpāmoa Formation: (top) Welcome Bay, Wharo and Otawera ignimbrite succession at Wharo Pā; (bottom) bluffs of Arateka Ignimbrite near Waitao Road. Note the inversion of relief. Yellow stars in stratigraphic columns and photos (where relevant) indicate approximate sampling positions. Grain size abbreviations in columns (B) and (C) follow nomenclature defined by White and Houghton (2006): f.A, fine ash (< 1 mm); c.A, coarse ash (0.5-1 mm); L, lapilli (2-64 mm); B, blocks/bombs (>64 mm).

Zircon crystals for dating were obtained from a bulk sample collected from the Aongatete River. A second sample collected from an outcrop at McLaren Falls, 20 km to the southwest **(Fig. 2a)**, was unsuitable for glass analysis because of extensive devitrification, but zircons were extracted for dating.

2.1.2 Ignimbrites of the Pāpāmoa Formation

The Pāpāmoa Formation is a complex package of pyroclastic flows **(Fig. 4b)** and interbedded fall deposits confined to the northern and western foothills of the Pāpāmoa Range where it overlies andesite and dacite lavas of the Otawa Formation (Briggs *et al.*, 2005). Briggs *et al.* (1996) divided the formation into the upper and lower ignimbrite units which are dated at 1.9 ± 0.1 Ma and 2.4 ± 0.02 Ma, respectively (Briggs *et al.*, 2005). A recent review of the internal stratigraphy of the Pāpāmoa Formation demonstrated that the formation is comprised of the deposits from several discrete eruptive events including the Arateka, Welcome Bay and Wharo ignimbrites (previously referred to as the Upper and Lower Pāpāmoa ignimbrites, respectively, (Briggs *et al.*, 1996), and the newly recognised Otawera ignimbrite which are described below.

Welcome Bay Ignimbrite

The Welcome Bay Ignimbrite is up to 115 m thick and is the major ridge-forming rock of the northern Pāpāmoa Range **(Fig.2a)**. They type section is found at NZ Topo50 BD37 869 194 where the ignimbrite consists of a 1.2-m-thick, well sorted, massive, medium lapilli, pumiceous fall deposit overlain by 115 m of creamy grey-beige, massive, pumice- and lithic-rich (30% and 15%, respectively), moderately-welded ignimbrite. This ignimbrite was previously named the Lower Pāpāmoa Ignimbrite by Briggs *et al.* (1996), but is re-named here with the recognition of a second ignimbrite unit (Wharo Ignimbrite, see below) lying stratigraphically above it. Welding increases slightly towards the top of the ignimbrite which produces irregular bluffs 6–10 m high that can be traced across the valleys **(Fig. 5a)**.

The Welcome Bay Ignimbrite is distinctive with two distinct juvenile clast compositions. The dominant clast type is a white-coloured dacitic pumice (~67 wt. % SiO_2; Namaliu, 2021) with a mineral assemblage comprising plagioclase, hornblende, and pyroxene. Subordinate clasts of dark-grey coloured andesitic pumices (~61 wt. % SiO_2) are less common and contain plagioclase and pyroxene but lack hornblende. Magma mingling between these two end-members is evident in flow-banded clasts. Pumice clast size is typically med-coarse lapilli (32–64mm). Lithics are dominantly black to dark-grey andesite with subordinate clasts of pink rhyolite.

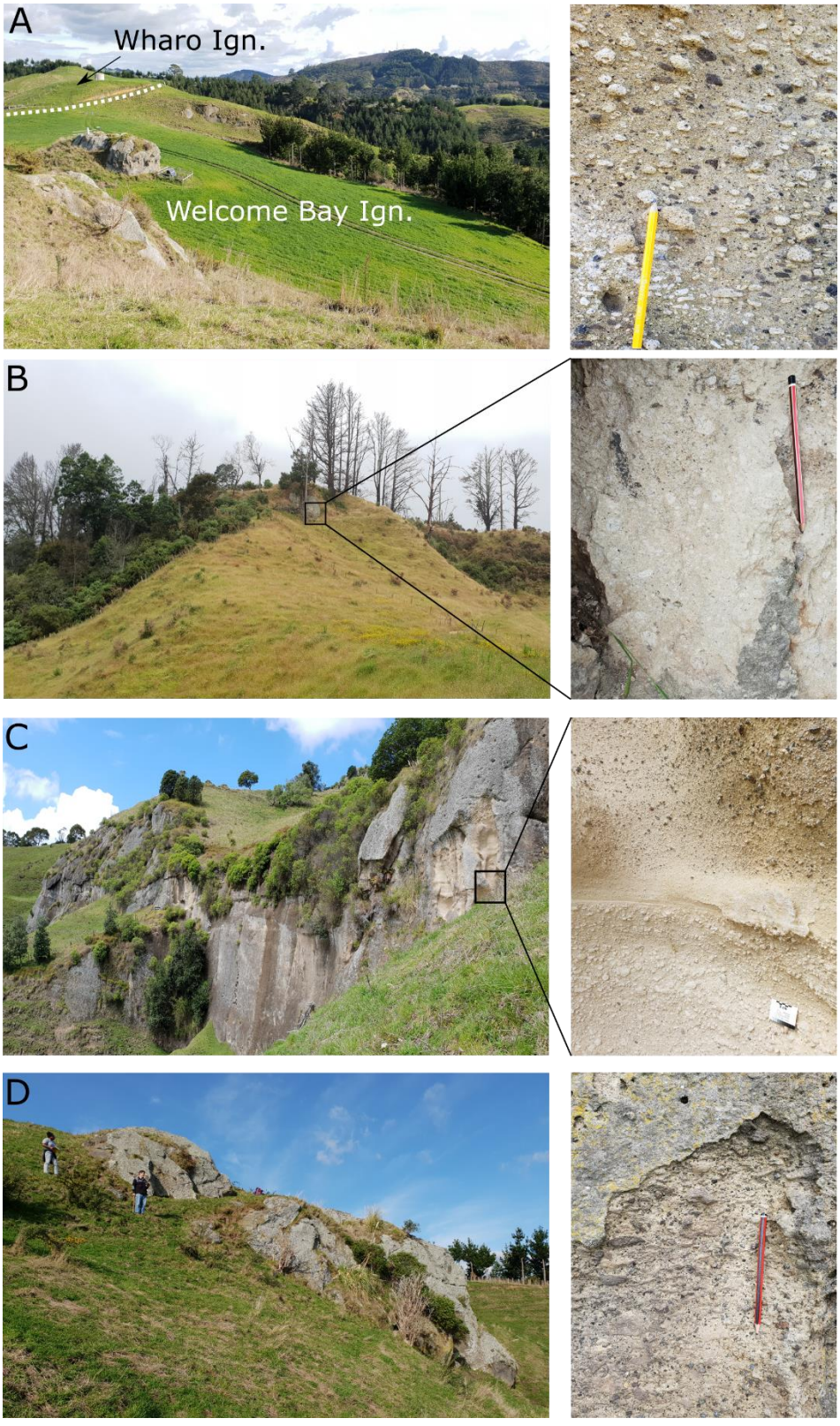

Figure 5. Photographs demonstrating typical outcrop features and textures of ignimbrites of the Pāpāmoa Formation. **(A)** Welcome Bay Ignimbrite in type region. Note bluffs on opposite (far) side of the valley, dark-grey pumice clasts (photo at right), and the overlying Wharo Ignimbrite. Contact lies at the base of the farm track. **(B)** Arateka Ignimbrite and (at right) white pumice clasts. **(C)** Otawera Ignimbrite and the contact between flow units 1 and 2. **(D)** Outlier bluffs of Wharo Ignimbrite. Note the distinct dark coloured fiamme and casehardening.

Wharo Ignimbrite

Overlying the Welcome Bay Ignimbrite is the Wharo Ignimbrite, a dark-grey, eutaxitic ignimbrite that infills paleo-valleys and forms caps on the top of some ridges. The type section is at the same location as the Welcome Bay Ignimbrite (i.e. NZ Topo50 BD37 869 194). The Wharo Ignimbrite was previously included as an upper unit within the Lower Pāpāmoa Ignimbrite, but has been renamed here on the basis of stratigraphic relationships, texture, and geochemical composition (Namaliu, 2021). Bluffs are commonly case-hardened, forming outliers up to 10 m high in the upper portions of valleys formed within the Welcome Bay ignimbrite **(Fig. 5d)**. Fiamme are dominated by plagioclase ± quartz, hornblende, pyroxene, and rare biotite.

Arateka Ignimbrite

The Arateka Ignimbrite is a cream-grey, massive, pumice-rich (20%), moderately-welded ignimbrite **(Fig. 5b)** and is equivalent to the Upper Pāpāmoa Ignimbrite of Briggs *et al.* (1996) that was dated at 1.9 ± 0.1 Ma (Briggs *et al.*, 2005). The type locality has previously been identified at NZ Topo50 BD37 944 777 (Hughes, 1993), where bluffs c. 60 m high crop out along Waitoa Road **(Fig. 2a)**. Pumice clasts are typically fine to med-lapilli in size with phenocrysts of plagioclase, hornblende, and resorbed pyroxene. Highly resorbed fragments of quartz are also present in a vitroclastic matrix.

Otawera Ignimbrite

The non-welded Otawera Ignimbrite is composed of multiple flow units and is found forming a 30 m high outlier bluff in the valley below Wharo Pā **(Figs. 2a and 5c)**. The type location is at NZ Topo50 BD37 881 197. It is also found cropping out in a similar manner at several locations throughout the central and western Pāpāmoa Range. It is radiometrically dated at 2.21 ± 0.13 Ma (Pittari *et al.*, 2021). This ignimbrite is generally fine grained (fine-mid lapilli), with lithic concentration zones at the base of flow units 1 and 2 that are dominated by andesitic and flow-banded rhyolite lavas. Phenocrysts constitute plagioclase and orthopyroxene with subordinate hornblende, rare quartz and juvenile clasts are set in a crystal-rich vitroclastic matrix.

Bulk samples for glass and zircon analysis were collected from the Welcome Bay, Wharo and Otawera ignimbrites (glass only) in the vicinity of Wharo Pā. Prominent bluffs of the Arateka Ignimbrite are visible along Waitao Road and were sampled from an outcrop near the top of the ridge **(Fig. 2a)**.

2.1.3 Te Puna Ignimbrite

The Te Puna Ignimbrite, formally defined by Briggs *et al.* (1996), is a non-welded, crystal-rich ignimbrite found in coastal sections around western areas of the Tauranga Harbour and the harbour side of Matakana Island. The thickest exposures are found at the type section along Te Puna Station Road

(NZ Topo50 BD36 725 239) where the ignimbrite forms a terrace >16 m thick **(Fig. 2a)**. Glass and zircons were separated from a bulk ignimbrite sample collected from a road cutting near the base of the ignimbrite forming this terrace. Phenocrysts include plagioclase, quartz, hornblende, orthopyroxene and biotite which has a distinctive golden colour. The Te Puna Ignimbrite has an $^{40}Ar/^{39}Ar$ age of 0.929 ± 0.012 Ma and is inferred to be a distal ignimbrite which flowed into the Tauranga region from Mangakino Volcanic Centre (MVC) **(Fig. 1)** (Briggs *et al.*, 2005; Leonard *et al.*, 2010; Cunningham *et al.*, 2016).

2.2 *Early Quaternary tephrostratigraphy of northern Hawke's Bay*

Numerous tephra beds are preserved in terrestrial, marginal-marine to marine rocks of the 2.4 to 1.63 Ma-aged Esk and lower Petane formations of northern Hawke's Bay, which crop out extensively within the valleys of the Mangaone, Esk, and Waikoau rivers, and in the Lake Tūtira area **(Fig. 2b)** (Bland *et al.*, 2007). The regional stratigraphy is summarised in **Fig. 6.** The Esk Mudstone Formation is punctuated by numerous tephra beds and is conformably overlain by sandstone to greywacke conglomerates of the lower Petane Formation. Sharply overlying the conglomerates is the Hikuroa Pumice Member. The Hikuroa Pumice Member has previously been correlated to an offshore tephra deposit in core OPD 1124C (Bland *et al.*, 2007) which corresponds to tephra AT-313 of Carter *et al.* (2004). Hopkins and Seward (2019) presented zircon fission-track ages for the Hikuroa Pumice Member at Darkys Spur of 2.0 ± 0.6 and 1.9 ± 0.4 Ma, which overlap within error with the paleomagnetic (2.165 Ma) and biostratigraphic (2.1496 Ma) ages of Stevens (2010). The Hikuroa Pumice Member within the Petane Formation **(Fig. 6b)**, and the two tephras Esk Mst-T1 and Esk Mst-T2 contained within the Esk Mudstone Formation **(Fig. 6c)**, are therefore chronologically equivalent to eruptive deposits of the Tauranga Volcanic Centre. More detailed descriptions of the Hikuroa Pumice Member, and Esk Mudstone tephras, Esk Mst-T1 and -T2, and sampling, are given below.

2.2.1 Hikuroa Pumice Member

The Hikuroa Pumice Member is a prominent non-welded, basal primary ignimbrite overlain by reworked pumiceous ash and lapilli, and capped by a highly fossiliferous shell and pebble bed. Exposures can be found along Darkys Spur, Beattie Road and MacIntyre Access Road **(Fig. 2b, and Fig. 56b)**.

The deposit is best exposed at Darkys Spur where the unit is over 9 m thick **(Fig. 7)**. A basal, normally-graded, laterally continuous, crystal-rich coarse ash underlies the lower 1.6 m of ignimbrite with

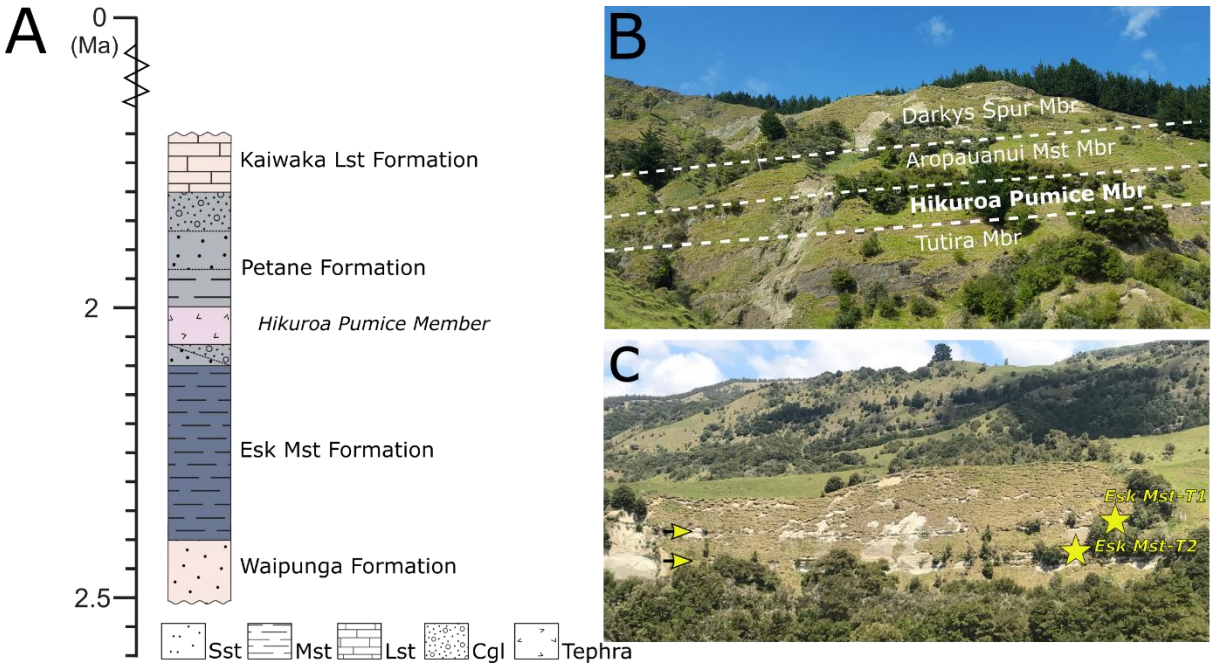

Figure 6. (A) Simplified stratigraphy and lithofacies of Early Quaternary marine sedimentary deposits in northern Hawke's Bay in the Lake Tūtira, Darkys Spur and Waikoau River areas **(Fig. 2b)**. Lithofacies of the Petane Formation are simplified to key lithologies of the repeating sequences (see Bland *et al.*, 2007, for full details). Lithological abbreviations are as follows: Sst, sandstone; Mst, mudstone; Lst, limestone; Cgl, conglomerate. **(B)** Annotated photo of outcrop at Darkys Spur. Mbr, Member. **(C)** Tephra-fall units Esk Mst-T1 and Esk Mst-T2 (yellow arrows) in the Esk Mudstone Formation, Waikoau River section. Approximate sampling positions indicated by yellow stars.

centimetre-scale horizontal stratification or low-angle (~10°) cross-stratification of very fine and coarse fine ash with occasional very fine to fine pumice lapilli layers. Primary depositional structures are overprinted by secondary deformation structures which present as convolute laminations where individual laminae can be traced through multiple folds and load casts. The upper 5.5 m consists of massive or centi- to decimetre-stratified, very-poorly to poorly sorted, fine-grained matrix-supported (fine-coarse ash to medium-fine ash) ignimbrite. This upper unit is overlain by a further 2.5 m of reworked volcaniclastic sediment dominated by fine ash and up to medium-lapilli-sized pumice clasts and carbonaceous fragments. An upper shell bed with rounded greywacke pebbles and cobbles, and disarticulated and broken bivalve and cockle shells overlies the Hikuroa Pumice Member.

The exposures at Beattie and MacIntyre Access roads were 1.75 m and ~7 m thick, respectively. Both outcrops show the same depositional and post-depositional structures in the lower 1.6 m below massive or stratified ignimbrite, reworked volcaniclastic sediments, and the capping shell bed. Charcoal fragments were prominent at the McIntyre Access Road outcrop and were found both in the overlying reworked volcaniclastic sediments and within the basal primary ignimbrite.

Glass samples were collected from multiple stratigraphic heights throughout deposits of this distal-ignimbrite at all three locations. Zircons for dating were collected from the basal crystal-rich coarse ash at Darkys Spur.

2.2.2 Esk Mudstone tephras

The Esk Mudstone Formation is exposed within the cliffs of the Waikoau River from approximately 3 km downstream from Waikoau Road to MacIntyre Access Road, off SH2, south of Lake Tūtira (Fig. 1c). The Waikoau River has extensively cut into the soft Esk Mudstone creating steep-sided cliffs up to 70 m high. The upstream section is located on the eastern cliff face of a large meander bend **(Fig. 6c)** where the base of the Esk Mudstone sits sharply above sandstone comprising the Waipunga Formation a few metres above the present river level. In the upper parts of the section, the blue-grey siltstone is punctuated by the two prominent tephra-fall beds, Esk Mst-T1 and T2, spaced 8 m vertically apart. The lower tephra (Esk Mst-T2) is 40 cm thick and consists of light-grey, coarse-ash. In contrast the upper tephra (Esk Mst-T1) consists of very fine, white-coloured ash and is 19 cm thick. Both tephra units have sharp, planar, basal contacts with the underlying siltstone, and are normally graded and bioturbated in upper parts. Bulk samples for glass and zircon analysis were collected from the lower 10to 15cm of each unit to minimise the presence of detrital glass shards or zircon which may have been introduced into the tuffs by bioturbation after deposition.

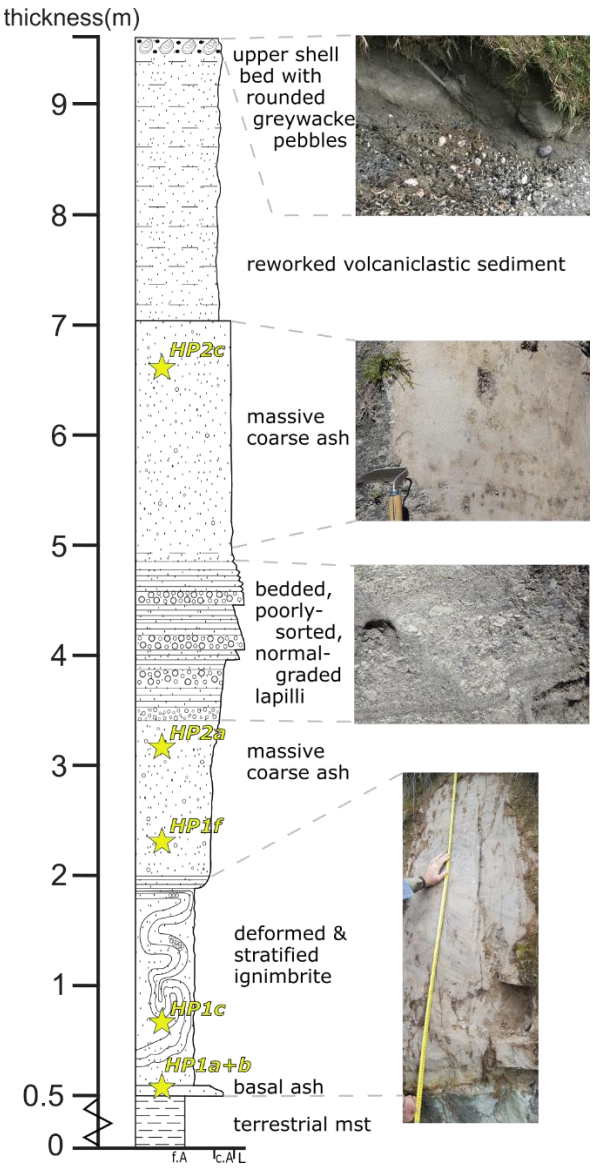

Figure 7. Stratigraphic log and outcrop photographs of Hikuroa Pumice Member at Darkys Spur, Hawke's Bay. Grain size abbreviations as in Figure 2. Samples collected for further analysis are highlighted by yellow stars.

3. U-Pb dating and characterisation of glass shards

3.1. U-Pb zircon dating

Zircons were concentrated from seven tephra-fall and ignimbrite samples for U-Pb geochronology. Separation methods included standard rock crushing (to 250 µm) with heavy minerals concentrated using a Gemini table and heavy liquid (sodium polytungstate, ρ = 2.8-3.0 g cm^{-3}) followed by magnetic separation using a Frantz isodynamic magnetic separator (10° incline, 15° forward tilt, 0.5 A). Individual crystals for analysis were hand-picked using a binocular microscope from the non-magnetic fraction, mounted in epoxy blocks, ground and polished to reveal internal sections. U-Pb ages were determined by laser ablation, inductively coupled, plasma mass spectrometry (LA-ICP-MS) at the

School of Science facility, University of Waikato, Hamilton, using an Agilent 8900 Triple Quadrupole ICP-MS coupled with a Laurin Technic S155 SE ablation cell and a RESOlution 1963 nm ArF excimer laser. Atomic masses Si29, Ti48, Y89, Zr91, Hf177, Pb204, Pb206, Pb207, Pb208, Th232, U235, and U238 were measured using a spot size of 30 µm with total ablation time of 45 s with a gas blank/background measurement of 15 s. The primary reference material GJ-1 and secondary reference zircon Temora-2 were analysed twice, both at the beginning and end of each run with two additional analyses of GJ every 10 unknowns. Data processing was performed using Iolite™ (V3) software package (Paton *et al.*, 2011) using the VizualAge data reduction scheme (Petrus & Kamber, 2012). Individual grain age determinations provided in the **supplementary material (SM8)** are $^{206}Pb/^{238}U$ dates that have been corrected for common Pb using the ^{207}Pb method (Williams, 1998) and Pb isotope evolution model of Stacey and Kramers (1975). Uranium decay constants and the $^{238}U/^{235}U$ ratio used are those recommended by Steiger and Jäger (1977). Correction for initial ^{230}Th-disequilibrium follows the method of Schärer (1984), using a Th/U magma ratio of 3 ± 1 (Sagar *et al.*, 2019), and a ^{230}Th decay constant of 9.1705 ± 0.0138 (Cheng *et al.*, 2013). Error-weighted mean ages and mean square weighted deviations (MSWD) were calculated using IsoplotR (Vermeesch, 2018) where discordia ages on Terra-Wasserburg plots were corrected using an anchored projection from a mean $^{207}Pb/^{206}Pb_c$ (0.836), and for initial ^{230}Th disequilibrium using a mean $f = (Th/U_{zircon})/(Th/U_{magma})$. Older zircon grains were excluded until MSDW values fell within acceptable limits relative to *N,* determined using the formula $1 + 2\sqrt{2/(n-1)}$ (Spencer *et al.*, 2016).

3.2. Glass composition

Glass-shard separates from the unconsolidated tephra-fall deposits and non-welded proximal and distal ignimbrites were obtained through disaggregation, sieving and magnetic separation before being mounted in epoxy resin and polished. Glass analysis of welded proximal ignimbrites were conducted using polished thin sections because the separation of individual juvenile clasts for analysis was not possible. Matrix glass was analysed to enable consistent comparison between both proximal and distal deposits.

In situ major element analyses by electron probe microanalysis (EPMA) was undertaken on individual glass shards using a JEOL JXA 8230 Superprobe at Victoria University of Wellington. A beam diameter of 10 µm at 8 nA and 15 kV accelerating voltage, was used to analyse major elements as oxides (SiO_2, TiO_2, Al_2O_3, $FeO_{(t)}$, MgO, MnO, CaO, Na_2O, and K_2O), along with Cl. During analysis, stage co-ordinates and back-scattered electron images of the shards were taken to allow the relocation of the analysis spots for subsequent LA-ICP-MS analysis. The matrix-matched standard VG-568 was used as a bracketing standard and run twice every 25 to 30 unknowns to monitor and correct for instrumental drift. Analytical totals for unknown glasses were between 92 and 99%, with deviations from 100% attributed to the omission of volatiles (predominately water) and non-analysed minor or trace

elements (Lowe *et al.*, 2017). Major elements are normalised by recalculating to 100% on a volatile-free basis. Accuracy of the analyses are within 3% of the recommended values for VG-568, with the exception of MnO, TiO_2, and Cl, which had offsets of 8.4%, 10%, and 8.24%, respectively. Analytical precision (2σ) is 1.30–1.43 wt % for SiO_2 and Na_2O and <0.3 wt % for all other major elements.

In-situ trace elements were analysed by the same LA-ICP-MS set up as described above. Data was acquired using a static spot method with spot sizes of 15 µm, and an ablation time of 40 s at 5 Hz. The standards ATHO-G and NIST-612 were run twice at the beginning and end of each session and every 10 unknowns. All data were reduced off-line on Iolite(TM) (V3), using ^{29}Si as the internal standard with NIST-612 as the calibration standard and ATHO-G as an independent secondary standard. Data was corrected for elemental fractionation as described by Pearce *et al.* (2011). Analytical precision (2σ) of analyses of ATHO-G is <5 with the exceptions of Cu, Rb, Sr, Y, Ce and Nd (2σ = 6–10), Ni (2σ = 20) and Zn, Zr and Ba (2σ = 35–92). The accuracy for all elements is <3 %. Refer to **supplementary material (SM2-5)** for the full dataset and standard comparisons.

4. Results

4.1. Zircon U-Pb ages

New zircon U-Pb ages for the two Esk Mudstone tephras, Esk Mst-T1 and -T2, and the Hikuroa Pumice Member (from northern Hawke's Bay), and for six samples derived from the five ignimbrites in Tauranga, are presented in **Table 1** and **Fig. 8**. Average U-Pb ages are crystallisation ages of the youngest zircon phenocryst population and provide a maximum eruption age for the eruptive deposits.

MSWD values indirectly assess the degree to which the weighted average and associated uncertainty represents a single population. If MSWD is >1, it is typically assumed that the data do not represent a single population, or if <1, the associated uncertainty may not fully represent the variation in the data set (Spencer *et al.*, 2016). Most of the age determinations for our study produced MSWD values of around 1 and thus are within the calculated range that indicates a single population at the 95% confidence level.

The ignimbrites erupted from the TgaVC range in age from 2.31 ± 0.046 Ma (Welcome Bay Ignimbrite) to 2.09 ± 0.029 Ma (Waiteariki Ignimbrite at McLaren Falls). The newly-defined ignimbrites of the Pāpāmoa Formation have ages of 2.31 ± 0.046 Ma (Welcome Bay Ignimbrite), 2.26 ± 0.046 Ma (Wharo Ignimbrite) and 2.25 ± 0.044 Ma (Arateka Ignimbrite). These ages are consistent with previous age determinations for the formation of 2.4 ± 0.02 Ma to 1.9 ± 0.1 Ma (Lower and Upper Pāpāmoa ignimbrites respectively, Briggs *et al.*, 2005) and 2.21 ± 0.13 for the Otawera Ignimbrite (Pittari *et al.*, 2021). However, the previously determined age for the (former) Upper Pāpāmoa Ignimbrite (1.9 ± 0.1 Ma) is younger than the date obtained for the newly-defined, equivalent Arateka Ignimbrite in our

study of 2.25 ± 0.044 Ma. Two age determinations for the Waitewhiki Ignimbrite were 2.18 ± 0.031 Ma (Aongatete River) and 2.09 ± 0.029 Ma (McLaren Falls), which overlap within error of each other and provide an average maximum age for this eruption of 2.1 Ma. The Te Puna Ignimbrite is dated at 1.1 ± 0.046 Ma, which is outside the age range for known volcanic activity of TgaVC and consistent with the inference that it is a distal ignimbrite derived from MVC (85 km SW of Tauranga) rather than a TgaVC origin (Briggs *et al.*, 2005).

Table 1: Summary of weighted average U-Pb zircon ages of five ignimbrites in TgaVC and of the Esk-Mudstone tephras T1 and T2, and Hikuroa Pumice Member, northern Hawke's Bay.

Geological formation/group	Pyroclastic unit (sample number)[1]	Age (Ma)	2σ error	N[2]	MSWD[3]
Pakaumanu Group	Te Puna Ignimbrite (TePu)	1.11	0.046	32	0.1
Petane Formation	Hikuroa Pumice Member (HP1&2)	2.13	0.029	48	1.0
Waitewhiki Formation	Waitewhiki Ignimbrite: McLaren's Falls (Wai#2)	2.09	0.029	49	1.2
	Waitewhiki Ignimbrite: Aongatete River (Wai22)	2.18	0.031	54	1.1
Pāpāmoa Formation	Otawera Ignimbrite[4]	2.21	0.13	na	na
Esk Mudstone Formation	Esk Mst-tephra (Esk Mst-T1)	2.22	0.088	47	0.8
	Esk Mst-tephra (Esk Mst-T2)	2.23	0.026	45	1.2
Pāpāmoa Formation	Arateka Ignimbrite (Pap4)	2.25	0.044	36	1.1
	Wharo Ignimbrite (Pap1)	2.26	0.046	41	1.0
	Welcome Bay Ignimbrite (Pap2)	2.31	0.046	31	0.84

[1]Sample location information provided in **supplementary material (SM1)**

[2]*N* = number of individual zircon grains contributing to the weighted average age

[3]MSDW = mean square weighted deviation. Acceptable limits relative to *N* were determined using the formula outlined in the text. Individual grain age determinations are provided in **supplementary material (SM8)**

[4]Age reported in Pittari et al. (2021)

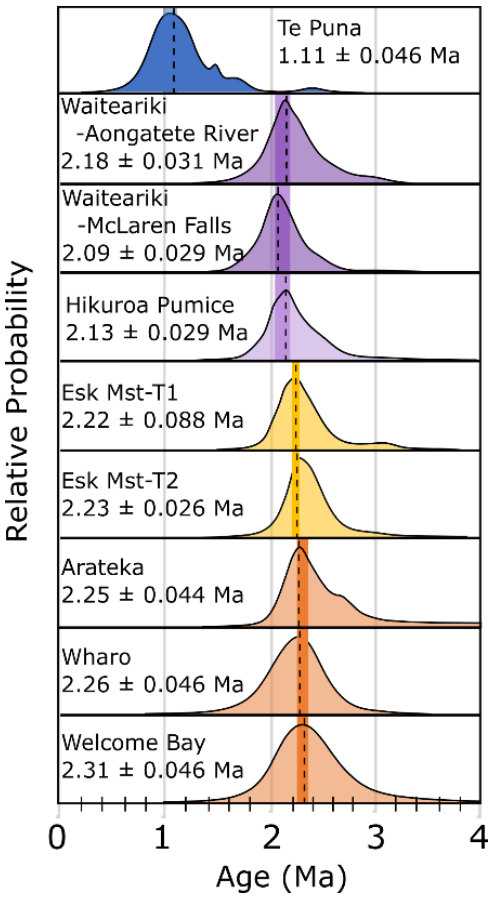

Figure 8. Probability density function plots of U-Pb zircon ages for four ignimbrite deposits in Tauranga, and of Hikuroa Pumice Formation and Esk Mst-T1 and -T2 tephras in Hawke's Bay, as dated in this study. Preferred average youngest-population zircon crystallisation ages are represented by the dashed lines (see also Table 1). Shaded bars represent the range of ages determined for the each of the formations. Note the overlapping age bars for Esk Mudstone tephras and for Welcome Bay, Wharo, and Arateka ignimbrites (see text for discussion).

The Esk Mudstone tephras have ages of 2.23 ± 0.026 Ma (Esk Mst-T2) and 2.22 ± 0.088 Ma (Esk Mst-T1) which overlap within error and cannot be distinguished on the basis of radiometric age alone. The two tephras, however, are separated stratigraphically by 8 m of blue-grey siltstone which means that Esk Mst-T1 is younger than Esk Mst-T2 and, therefore, that a period of time elapsed between the two eruptions. The Hikuroa Pumice Member stratigraphically overlies the Esk Mudstone and the sandstone to greywacke conglomerates of the lower Petane Formation. The Hikuroa Pumice Member is dated here at 2.13 ± 0.029 Ma an age that is consistent with a biostratigraphic age of 2.14 Ma (Stevens (2010) and two previously-published (but less precise) zircon fission-track ages of 1.9 ± 0.4 Ma and 2.0 ± 0.6 Ma (Hopkins & Seward, 2019).

4.2. Glass composition

Representative major and trace element compositions of glass shards from ignimbrite and tephra-fall units are presented in **Table 2**, with the full dataset available as **supplementary data (SM5)**.

Table 2: Major and trace-element analyses of glass shards in tephra-fall and ignimbrite deposits from Hawke's Bay and TgaVC. Major-element oxide values in wt % (± 2σ for *n* analyses) are normalised to 100% volatile free; trace-element values are in ppm (± 2σ for *n* analyses); *n* = number of individual glass shards analysed for major/minor elements (EPMA) and trace elements (LA-ICP-MS). **See supplementary material SM5** for full dataset.

Sample no.	Esk Mst-T1				Esk Mst-T2		HP1 & 2		HP3		HP4		WAI22	
Formation	Esk Mudstone				Esk Mudstone		Hikuroa Pumice – Darkys Spur		Hikuroa Pumice – MacIntyre Access Rd		Hikuroa Pumice – Beattie Rd		Waitewhio Ignimbrite[2] Core ES112	
Major elements as oxides (wt %) (2σ errors)														
	Population1		*Population2*											
SiO_2	73.93	(0.20)	77.14	*(0.44)*	75.60	*(0.34)*	77.33	*(0.37)*	77.28	*(0.32)*	77.34	*(0.39)*	77.53	*(0.39)*
Al_2O_3	13.67	(0.55)	12.82	*(0.21)*	13.40	*(0.16)*	12.46	*(0.16)*	12.45	*(0.17)*	12.46	*(0.19)*	12.55	*(0.28)*
MgO	0.29	(0.05)	0.12	*(0.02)*	0.06	*(0.02)*	0.06	*(0.03)*	0.06	*(0.06)*	0.06	*(0.03)*	0.10	*(0.05)*
CaO	1.94	(0.09	1.17	*(0.07)*	1.28	*(0.03)*	0.89	*(0.11)*	0.92	*(0.17)*	0.89	*(0.12)*	1.01	*(0.18)*
TiO_2	0.26	(0.10)	0.08	*(0.02)*	0.10	*(0.04)*	0.08	*(0.03)*	0.09	*(0.04)*	0.08	*(0.02)*	0.09	*(0.04)*
MnO	0.03	(0.03)	0.03	*(0.03)*	0.04	*(0.03)*	0.04	*(0.04)*	0.04	*(0.04)*	0.04	*(0.05)*	0.03	*(0.03)*
FeO_t[3]	2.69	(0.51)	1.30	*(0.21)*	1.78	*(0.19)*	1.45	*(0.28)*	1.46	*(0.25)*	1.43	*(0.28)*	1.16	*(0.29)*
Na_2O	3.93	(0.16)	3.56	*(0.30)*	3.81	*(0.46)*	3.87	*(0.35)*	3.83	*(0.35)*	3.86	*(0.38)*	3.36	*(0.33)*
K_2O	3.13	(0.17)	3.65	*(0.38)*	3.86	*(0.44)*	3.69	*(0.41)*	3.73	*(0.44)*	3.70	*(0.54)*	4.06	*(0.38)*
Cl	0.17	(0.01)	0.18	*(0.02)*	0.10	*(0.01)*	0.19	*(0.02)*	0.20	*(0.02)*	0.20	*(0.02)*	0.17	*(0.05)*
Total	95.27	(0.60)	94.86	*(0.84)*	95.98	*(1.76)*	96.14	*(2.21)*	95.60	*(1.81)*	96.09	*(2.49)*	97.08	*(1.42)*
n	5		*7*		15		63		34		29		25	
Trace elements (ppm)[1] (2σ errors)														
Sc	7.27	*(4.87)*	2.42	*(1.02)*	8.40	*(4.98)*	5.78	*(1.98)*	5.19	(1.65)	5.55	*(1.67)*	3.30	*(1.45)*
V	15.30	*(8.88)*	2.80	*(1.52)*	3.57	*(1.40)*	2.60	*(6.38)*	1.97	(4.50)	3.83	*(9.07)*	2.72	*(1.68)*
Co	4.81	*(5.42)*	1.14	*(0.50)*	0.72	*(0.71)*	0.64	*(0.54)*	0.65	(0.50)	0.87	*(1.35)*	0.90	*(0.66)*
Cu	13.68	*(21.10)*	3.82	*(1.84)*	6.00	*(3.63)*	7.93	*(16.28)*	5.80	(15.03)	6.76	*(15.49)*	5.20	*(7.79)*
Zn	48.24	*(38.09)*	37.93	*(7.46)*	78.44	*(32.01)*	43.19	*(17.18)*	38.56	(20.12)	36.41	*(17.20)*	31.90	*(16.81))*
Ga	18.95	*(4.07)*	16.62	*(2.25)*	23.66	*(8.20)*	17.14	*(3.55)*	16.23	(3.15)	17.30	*(2.94)*	14.03	*(4.01)*
Rb	121.80	*(16.93)*	134.09	*(14.27)*	130.01	*(11.87)*	130.21	*(18.32)*	127.09	(17.23)	134.50	*(15.17)*	128.10	*(31.06)*
Sr	102.17	*(25.87)*	80.81	*(12.35)*	88.83	*(16.47)*	54.69	*(24.36)*	51.78	(21.35)	52.93	*(14.38)*	69.25	*(32.59)*
Y	16.48	*(15.47)*	14.90	*(4.15)*	29.11	*(6.58)*	24.56	*(8.92)*	21.19	(8.84)	23.58	*(7.93)*	17.63	*(5.73)*
Zr	153.45	*(99.03)*	85.88	*(18.56)*	145.77	*(21.38)*	113.05	*(39.75)*	101.63	(39.40)	108.21	*(34.10)*	89.22	*(29.21)*
Nb	5.83	*(2.87)*	5.56	*(0.70)*	7.58	*(0.92)*	8.00	*(0.99)*	7.29	(1.39)	7.83	*(1.48)*	5.38	*(1.78)*
Cs	5.45	*(0.89)*	6.43	*(0.65)*	6.70	*(0.95)*	6.08	*(0.96)*	5.79	(0.93)	6.19	*(1.05)*	5.95	*(1.73)*
Ba	614.80	*(144.91)*	786.97	*(94.94)*	759.03	*(128.86)*	817.68	*(136.57)*	770.53	(140.56)	801.73	*(155.62)*	813.16	*(228.45)*
La	16.50	*(7.28)*	20.51	*(4.58)*	24.13	*(4.10)*	22.81	*(5.64)*	21.11	(5.64)	22.80	*(5.04)*	22.30	*(6.21)*
Ce	40.87	*(11.79)*	42.49	*(5.63)*	55.80	*(10.60)*	49.43	*(10.55)*	45.44	(9.92)	49.51	*(9.87)*	44.25	*(11.72)*
Pr	4.18	*(2.12)*	4.10	*(0.98)*	6.21	*(1.52)*	5.34	*(1.28)*	4.89	(1.36)	5.25	*(1.33)*	4.64	*(1.33)*
Nd	18.82	*(9.06)*	14.84	*(2.46)*	24.90	*(6.27)*	20.16	*(5.57)*	17.79	(5.40)	19.83	*(5.76)*	16.48	*(5.24)*
Sm	2.86	*(2.23)*	2.48	*(0.97)*	4.91	*(1.91)*	4.31	*(1.54)*	3.64	(1.41)	3.97	*(1.47)*	3.01	*(1.25)*
Eu	0.49	*(0.73)*	0.41	*(0.24)*	0.58	*(0.33)*	0.53	*(0.31)*	0.48	(0.30)	0.53	*(0.28)*	0.41	*(0.19)*
Gd	2.89	*(3.52)*	2.40	*(1.14)*	5.07	*(2.02)*	4.05	*(1.75)*	3.39	(1.86)	3.72	*(1.63)*	2.81	*(1.19)*
Tb	0.47	*(0.28)*	0.36	*(0.16)*	0.77	*(0.30)*	0.63	*(0.28)*	0.58	(0.28)	0.59	*(0.32)*	0.46	*(0.17)*
Dy	2.76	*(2.86)*	2.11	*(0.76)*	5.35	*(1.54)*	4.22	*(1.51)*	3.61	(1.59)	3.76	*(1.46)*	2.83	*(1.10)*
Ho	0.55	*(0.65)*	0.44	*(0.16)*	1.04	*(0.33)*	0.82	*(0.37)*	0.76	(0.38)	0.82	*(0.31)*	0.60	*(0.24)*
Er	1.79	*(2.17)*	1.54	*(0.76)*	2.98	*(0.97)*	2.58	*(1.12)*	2.25	(1.35)	2.46	*(1.07)*	1.82	*(0.72)*
Tm	0.24	*(0.33)*	0.24	*(0.10)*	0.40	*(0.18)*	0.37	*(0.20)*	0.34	(0.19)	0.35	*(0.17)*	0.27	*(0.10)*
Yb	1.40	*(2.31)*	1.68	*(0.87)*	3.23	*(1.50)*	2.79	*(1.19)*	2.37	(1.39)	2.55	*(1.40)*	2.08	*(0.73)*
Lu	0.27	*(0.34)*	0.26	*(0.17)*	0.42	*(0.22)*	0.39	*(0.24)*	0.35	(0.22)	0.41	*(0.23)*	0.33	*(0.12)*
Hf	3.54	*(3.09)*	2.74	*(0.90)*	4.22	*(1.20)*	3.57	*(1.43)*	3.25	(1.40)	3.43	*(1.30)*	3.08	*(1.05)*
Ta	0.27	*(0.24)*	0.41	*(0.18)*	0.53	*(0.16)*	0.60	*(0.24)*	0.54	(0.22)	0.58	*(0.24)*	0.52	*(0.17)*
W	1.37	*(0.97)*	1.56	*(0.35)*	2.00	*(0.45)*	1.53	*(0.38)*	1.49	(0.45)	1.56	*(0.42)*	1.54	*(0.49)*
Pb	30.92	*(6.39)*	27.19	*(4.60)*	41.45	*(13.37)*	31.68	*(23.49)*	30.43	(16.62)	30.73	*(12.77)*	22.09	*(7.54)*
Th	5.98	*(5.40)*	10.47	*(3.31)*	10.50	*(2.39)*	10.41	*(4.19)*	9.22	(4.35)	10.08	*(3.57)*	11.75	*(3.50)*
U	1.90	*(0.69)*	2.89	*(0.72)*	2.76	*(0.64)*	2.83	*(0.75)*	2.56	(0.70)	2.77	*(0.74)*	2.89	*(0.84)*
N	*5*		*7*		15		63		34		29		22	

[1]Ni & Cr removed because of inconsistent analytical results

[2]McLaren Falls sample was not analysed for major and trace elements because of the lack of suitable glass. [3]Total iron expressed as FeO_t

Table 2: Continued

Sample no.	Te Pu		L11				L5		L12		L2WP/L4		L2BP/L7	
Formation	Te Puna Ignimbrite		Arateka Ignimbrite				Wharo Ignimbrite		Otawera Ignimbrite		Welcome Bay Ignimbrite			
Major elements as oxides (wt %) (2σ errors)														
			Population1		*Population2*									
SiO_2	76.94	*(0.37)*	73.57	(0.71)	77.02	*(0.08)*	71.51	*(0.91)*	76.09	*(0.36)*	77.02	*(1.13)*	74.72	*(2.78)*
Al_2O_3	12.37	*(0.13)*	13.74	(1.18)	12.47	*(0.20)*	14.42	*(0.60)*	12.66	*(0.18)*	12.72	*(0.54)*	13.10	*(0.82)*
MgO	0.09	*(0.05)*	0.30	(0.04)	0.11	*(0.01)*	0.41	*(0.16)*	0.05	*(0.03)*	0.08	*(0.06)*	0.20	*(0.19)*
CaO	0.81	*(0.20)*	1.93	(0.06)	1.16	*(0.00)*	2.49	*(0.34)*	0.89	*(0.10)*	1.23	*(0.21)*	1.71	*(0.62)*
TiO_2	0.09	*(0.05)*	0.33	(0.02)	0.09	*(0.01)*	0.38	*(0.04)*	0.11	*(0.03)*	0.09	*(0.03)*	0.25	*(0.23)*
MnO	0.03	*(0.03)*	0.07	(0.01)	0.02	*(0.02)*	0.08	*(0.03)*	0.03	*(0.03)*	0.02	*(0.03)*	0.04	*(0.03)*
FeO_t[3]	1.11	*(0.23)*	2.71	(0.13)	1.23	*(0.11)*	3.08	*(0.87)*	1.57	*(0.15)*	0.82	*(0.64)*	2.17	*(1.29)*
Na_2O	3.83	*(0.25)*	3.81	(0.44)	3.86	*(0.14)*	4.22	*(0.32)*	4.61	*(0.29)*	4.11	*(0.34)*	4.25	*(0.37)*
K_2O	4.05	*(0.19)*	3.36	(0.21)	3.84	*(0.15)*	3.29	*(0.34)*	3.80	*(0.17)*	3.75	*(0.23)*	3.40	*(0.32)*
ClO	0.26	*(0.03)*	0.17	(0.05)	0.19	*(0.01)*	0.13	*(0.03)*	0.18	*(0.02)*	0.14	*(0.09)*	0.16	*(0.05)*
Total	98.97	*(0.54)*	94.99	(4.35)	95.99	*(1.32)*	94.31	*(2.34)*	96.08	*(1.22)*	95.01	*(2.79)*	95.62	*(2.96)*
n	20		4		*2*		9		50		24		6	
Trace elements (ppm)[1,4] (2σ errors)														
Zn	39.29	*(9.33)*	168.43	*(123.34)*	52.51	*(7.12)*	86.70	*(104.04)*	58.97	*(27.22)*	40.50	*(37.88)*	58.21	*(39.67)*
Ga	15.13	*(4.65)*	33.06	*(18.91)*	19.09	*(0.00)*	32.91	*(53.87)*	19.59	*(9.65)*	18.87	*(6.59)*	22.26	*(5.28)*
Rb	153.76	*(17.33)*	110.53	*(33.47)*	131.68	*(24.81)*	121.56	*(21.50)*	140.89	*(21.70)*	142.05	*(24.84)*	120.44	*(22.06)*
Sr	53.19	*(19.14)*	76.90	*(25.29)*	66.29	*(30.60)*	158.91	*(31.77)*	57.54	*(15.70)*	83.66	*(35.04)*	92.81	*(50.01)*
Y	23.93	*(5.44)*	19.79	*(7.64)*	12.83	*(6.36)*	22.39	*(10.39)*	30.27	*(8.96)*	14.90	*(6.03)*	20.67	*(17.16)*
Zr	93.89	*(26.55)*	151.40	*(51.41)*	76.10	*(31.25)*	190.19	*(62.21)*	165.42	*(48.32)*	88.02	*(41.54)*	157.34	*(147.76)*
Nb	8.33	*(1.44)*	4.66	*(1.95)*	4.62	*(1.57)*	7.94	*(1.35)*	8.65	*(1.16)*	5.22	*(1.28)*	6.57	*(3.24)*
Cs	4.44	*(1.06)*	4.86	*(3.14)*	4.15	*(0.29)*	4.41	*(4.00)*	4.21	*(1.58)*	4.46	*(1.87)*	3.77	*(0.72)*
Ba	883.59	*(104.11)*	501.38	*(143.10)*	703.10	*(371.51)*	608.63	*(152.15)*	822.02	*(200.95)*	784.78	*(133.14)*	712.79	*(201.78)*
La	27.24	*(5.35)*	14.85	*(4.93)*	17.29	*(11.31)*	18.74	*(7.03)*	25.57	*(6.52)*	20.33	*(5.69)*	19.17	*(6.75)*
Ce	55.76	*(11.96)*	30.55	*(10.14)*	32.92	*(17.29)*	38.70	*(21.40)*	54.12	*(15.28)*	40.68	*(9.28)*	40.36	*(16.49)*
Pr	5.79	*(1.14)*	3.73	*(1.52)*	3.59	*(1.98)*	4.97	*(2.16)*	6.00	*(1.51)*	4.11	*(1.13)*	4.39	*(2.14)*
Nd	23.25	*(7.28)*	15.35	*(4.92)*	11.16	*(7.73)*	18.33	*(7.14)*	23.23	*(7.61)*	13.81	*(6.36)*	18.81	*(13.28)*
Sm	4.15	*(1.81)*	3.11	*(1.93)*	4.50	*(2.65)*	3.95	*(2.04)*	5.16	*(2.75)*	2.41	*(1.91)*	3.75	*(2.80)*
Eu	0.59	*(0.37)*	0.75	*(0.57)*	0.36	*(0.16)*	0.92	*(0.57)*	0.68	*(0.51)*	0.43	*(0.39)*	0.83	*(0.80)*
Gd	3.84	*(1.36)*	3.16	*(2.64)*	2.03	*(2.71)*	2.93	*(2.85)*	5.29	*(2.25)*	2.36	*(1.36)*	3.95	*(2.62)*
Tb	0.59	*(0.19)*	0.44	*(0.29)*	0.20	*(0.39)*	0.71	*(0.35)*	0.81	*(0.35)*	0.35	*(0.32)*	0.59	*(0.63)*
Dy	3.75	*(1.33)*	3.38	*(2.17)*	1.91	*(1.97)*	4.06	*(1.16)*	5.27	*(1.59)*	2.10	*(1.65)*	3.11	*(3.21)*
Ho	0.85	*(0.27)*	0.70	*(0.39)*	0.37	*(0.15)*	0.78	*(0.48)*	1.01	*(0.49)*	0.52	*(0.42)*	0.90	*(0.44)*
Er	2.52	*(1.25)*	2.05	*(1.09)*	1.32	*(0.76)*	2.58	*(1.62)*	3.13	*(1.28)*	1.58	*(1.32)*	2.01	*(1.74)*
Tm	0.39	*(0.24)*	0.19	*(0.25)*	0.39	*(0.00)*	0.39	*(0.24)*	0.44	*(0.28)*	0.24	*(0.21)*	0.34	*(0.38)*
Yb	2.87	*(1.51)*	2.45	*(0.60)*	1.66	*(0.62)*	2.85	*(1.80)*	3.35	*(1.62)*	2.19	*(1.67)*	3.01	*(2.07)*
Lu	0.48	*(0.27)*	0.40	*(0.21)*	0.24	*(0.00)*	0.39	*(0.21)*	0.50	*(0.30)*	0.35	*(0.30)*	0.53	*(0.28)*
Hf	3.39	*(0.65)*	3.47	*(1.55)*	2.04	*(1.58)*	4.54	*(2.81)*	5.01	*(1.38)*	2.65	*(1.42)*	4.29	*(3.26)*
Ta	0.87	*(0.45)*	0.32	*(0.26)*	0.42	*(0.28)*	0.61	*(0.49)*	0.65	*(0.25)*	0.47	*(0.31)*	0.40	*(0.41)*
W	5.07	*(26.98)*	1.50	*(0.94)*	2.10	*(1.18)*	1.91	*(1.56)*	2.10	*(2.27)*	1.60	*(0.80)*	1.66	*(0.69)*
Pb	27.25	*(4.99)*	28.28	*(12.05)*	21.06	*(8.91)*	37.67	*(40.87)*	30.07	*(8.69)*	29.95	*(11.80)*	22.12	*(10.46)*
Th	14.85	*(4.73)*	5.55	*(1.39)*	7.80	*(5.06)*	8.06	*(5.39)*	12.28	*(3.99)*	10.21	*(4.10)*	8.48	*(2.92)*
U	3.60	*(0.96)*	1.98	*(0.85)*	2.39	*(0.56)*	2.07	*(0.90)*	3.00	*(0.95)*	2.56	*(0.91)*	2.25	*(0.40)*
n	20		4		2		*8*		48		22		5	

[1]Ni & Cr removed because of inconsistent analytical results

[2]McLaren Falls sample was not analysed for major and trace elements because of the lack of suitable glass

[3]Total iron expressed as FeO_t

[4]Sc, V, Co, and Cu not analysed

All samples analysed have SiO_2 contents of between 69.4 and 77.4 wt. % (normalised basis) with K_2O values between 2.2-5.4 wt. %, thus classifying them as medium to high-K calc-alkaline rhyolites (Le Maitre *et al.*, 2002). Values for ratio SiO_2/K_2O and Na_2O+K_2O are between 14.4-25.2 and 6.8-8.2, respectively, a characteristic shared with other magmas erupted from pre- and early TVZ sources (Hopkins *et al.*, 2021b). Individual tephra horizons can often be distinguished from one another using a number of major element oxide bivariate plots, for example FeO_t vs. CaO or K_2O and SiO_2 vs. K_2O or Al_2O_3. For additional fingerprinting, trace element compositions (e.g. Zr vs Y, Rb and Sr) and trace element ratios were used (e.g. Zr/Y vs. Ba/Sr; or Rb/Sr and Zr/Nb vs Rb/Sr).

The Wharo, Otawera, Waiteariki and Te Puna ignimbrites, the Hikuroa Pumice Member and the Esk Mst-T2 tephra, all show homogenous major element glass compositions, typically within < ± 1 wt. % **(Figs. 9-11)**. In contrast, glass shards from the Esk Mst-T1 tephra, and the Arateka and Welcome Bay ignimbrites show bimodal major element populations, as depicted by relatively 'low' vs 'high' SiO_2 contents of 73.0–74.1 and 75.7–77.8 wt. %, respectively **(Fig. 9)**. Consistent groupings can also be distinguished in CaO, FeO_t, K_2O, Al_2O_3 and MgO along with bivariate plots of trace-element ratios where the low SiO_2 population has higher abundances of CaO (+ 1.0 wt. %), FeO_t (+ 1.5 wt. %), K_2O (+ 1.0%) but lower Ba/Sr and higher Zr/Y ratios (-4 and +1-3, respectively). Zr/Y vs Ba/Sr trace element ratios also suggest heterogeneity within the Hikuroa Pumice Member **(Fig. 10f)**. Mixed-shard populations may result from variations in magma composition (Naish *et al.*, 1996; Kilgour & Smith, 2008; Cooper *et al.*, 2012), or post- or syn-depositional reworking (Schneider *et al.*, 2001; Lowe *et al.*, 2017), and possible causes for mixed populations are discussed further below.

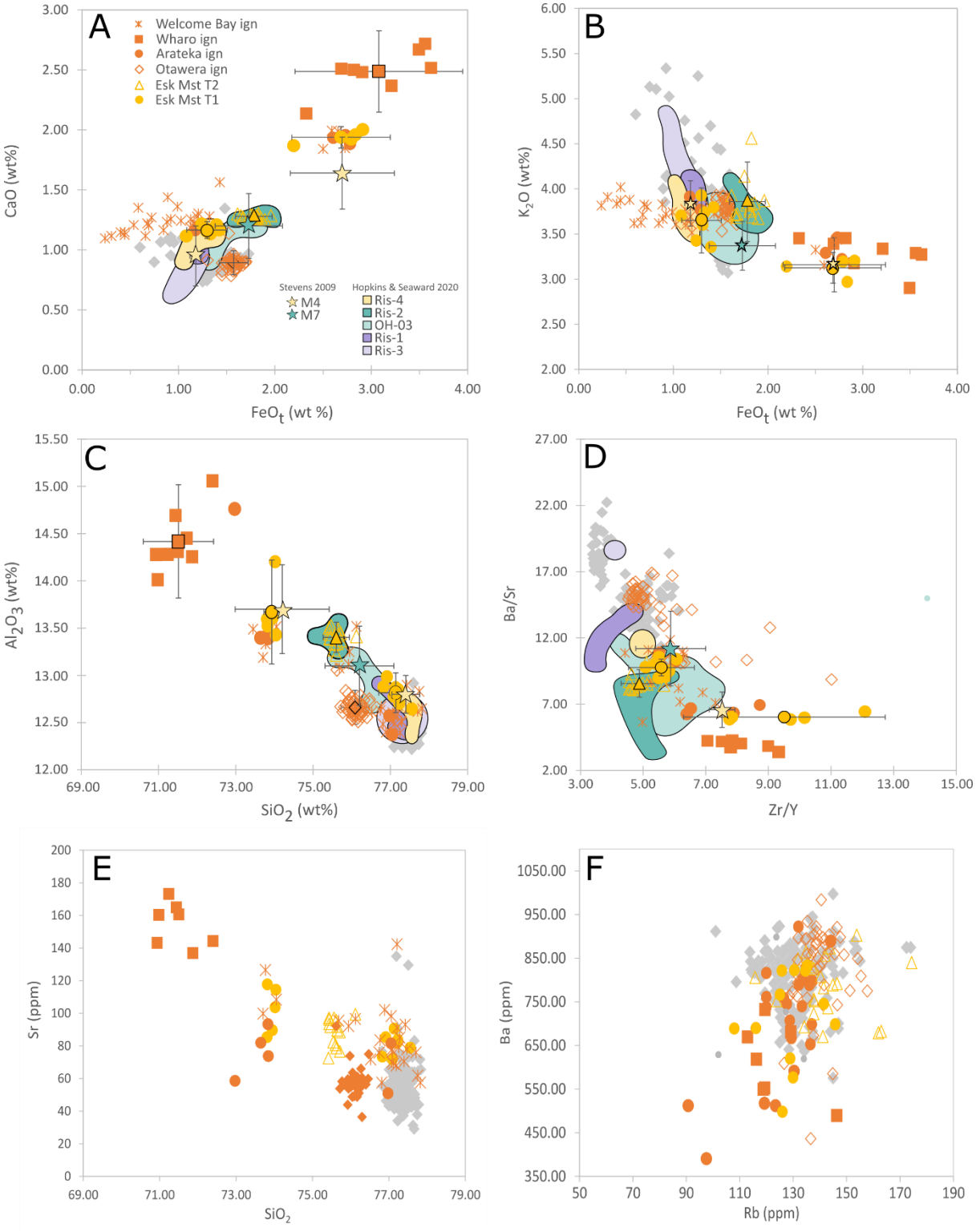

Figure 9. Representative bivariate plots of analyses including means (± 2σ error bars) of selected major elements (as oxides, normalised to 100% volatile free) and trace element ratios of glass from four proximal ignimbrites in TgaVC (Arateka, Welcome Bay, Wharo, and Otawera) and from the Esk-Mudstone tephras T1 and T2. Distal correlatives are shown as coloured polygons, representing so-called Rissington tephras (Ris, OH) of Hopkins and Seward (2019), and ODP 1124 tephra horizons of Stevens (2010) as stars (see Section 6). Grey diamonds represent Waitea riki Ignimbrite and Hikuroa Pumice glass analyses (see Figure 10 for details).

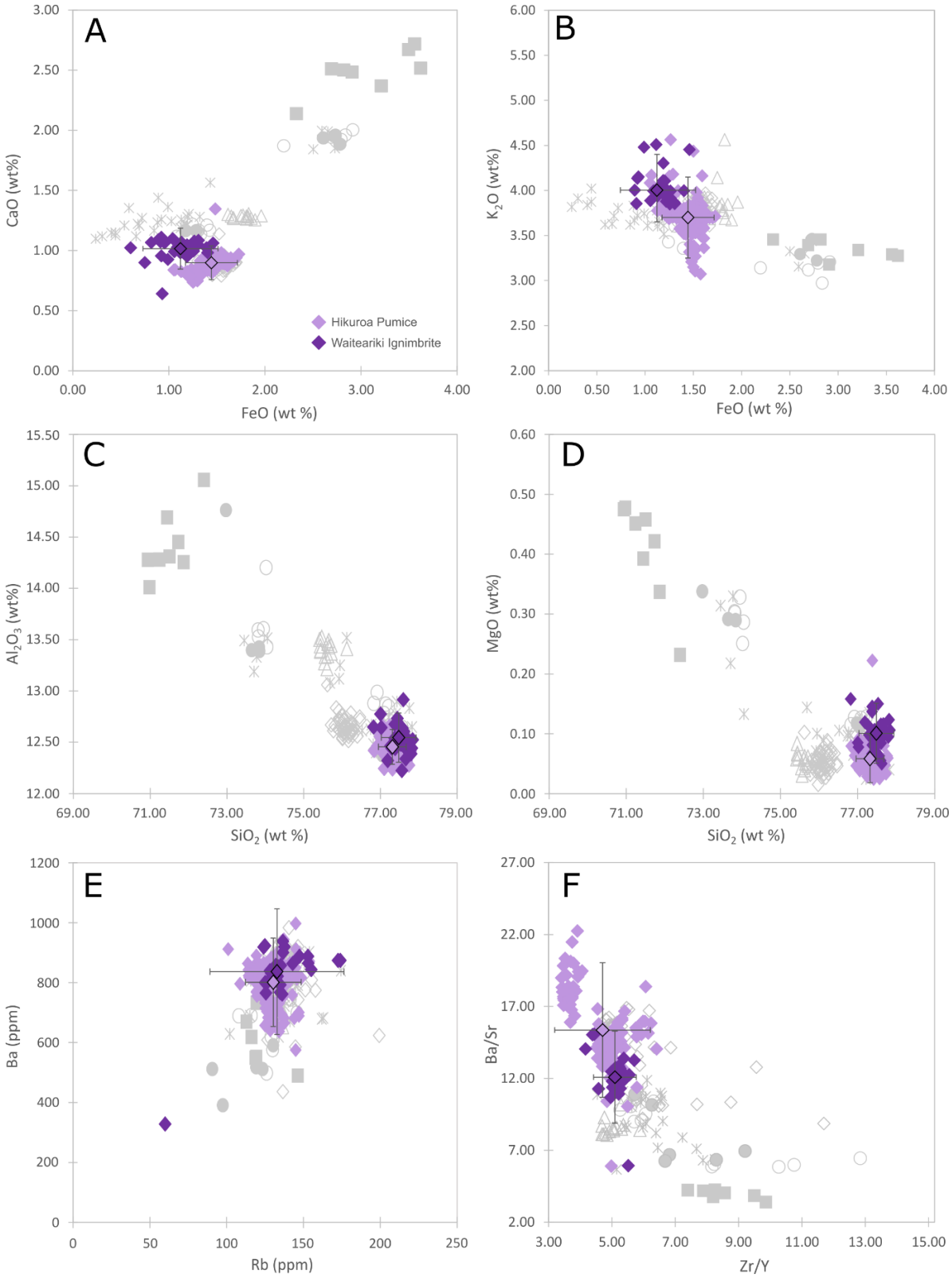

Figure 10. Representative bivariate plots of analyses including means (black outline with ± 2σ error bars) of selected major elements (as oxides, normalised to 100% volatile free), trace elements and trace element ratios, of glass from the Waiteariki Ignimbrite and Hikuroa Pumice Member. Other proximal ignimbrites in the TgaVC (Arateka, Welcome Bay, Wharo, and Otawera) and the Esk-Mudstone tephras, Esk Mst-T1 and -T2 are shown in grey (as per Figure 9).

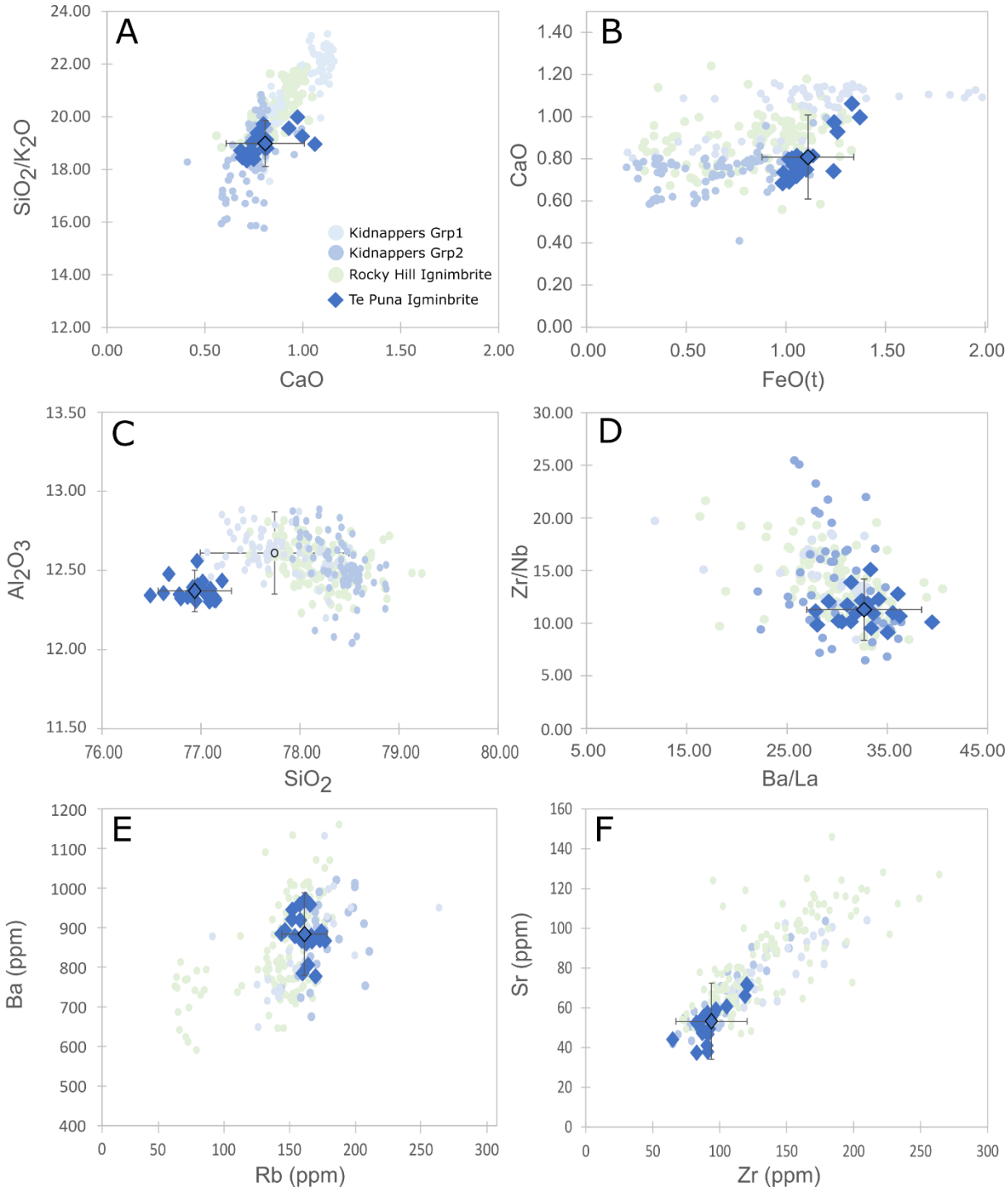

Figure 11. Bivariate plots of analyses including mean (± 2σ error bars) of glass of Te Puna ignimbrite (this study) compared with analyses of Kidnappers and Rocky Hill ignimbrites (data from Cooper *et al.* 2016). Major elemental data (as oxides) all on normalised basis.

5. Discussion

5.1. Correlations

Using the new U-Pb zircon ages and glass compositional data, together with stratigraphic considerations, correlations between the TgaVC-derived ignimbrites and the Hikuroa Pumice Member and Esk-Mudstone tephras T1 and T2, and the MVC-derived Te Puna Ignimbrite, are made with other previously identified horizons both onshore and offshore **(Table 3)**.

5.1.1 Proximal ignimbrites from TgaVC and Esk-Mudstone tephras T1 and T2

The U-Pb zircon ages of the Arateka and Wharo ignimbrites overlap with those of the Esk-Mudstone tephras T1 and T2 **(Fig. 8; Table 1)**, and of the Otawera Ignimbrite, meaning all three are potential correlatives for the two Esk-Mudstone tephras on the basis of their similar age. Stratigraphic field relationships and an older zircon crystallisation age of 2.31 ± 0.046 Ma for the Welcome Bay Ignimbrite indicates it is unlikely to be a correlative of Esk-Mudstone tephras T1 and T2. The Otawera Ignimbrite (2.21 Ma) cannot be separated from the Aretaka, Welcome Bay, and Wharo ignimbrites on age alone, but stratigraphically it is younger than the Welcome Bay and Wharo ignimbrites **(Figs. 3, and 5b)**.

The Arateka, Welcome Bay, Wharo, and Otawera ignimbrites, although having broadly similar rhyolitic glass compositions, can nevertheless be discriminated on bivariate plots **(Fig. 9)**. The Welcome Bay and Arateka ignimbrites show bimodal geochemical populations, with the second population comprising glass with elevated contents of FeO_t, CaO and Al_2O_3, lower SiO_2 and K_2O contents, and higher ratios of incompatible trace elements, such as Zr/Y. This bimodality was not unexpected for the Welcome Bay Ignimbrite, because field specimens have both white and dark juvenile clasts of two distinct compositions and textual evidence for magma mixing (Namaliu, 2021). The Arateka Ignimbrite, however, contains only white pumice and no physical evidence for magma mixing was observed, yet the same two geochemical populations can be discerned in the glass compositions. The glass analyses of the Otawera and Wharo ignimbrites show distinct groupings separate from those of the Welcome Bay and Arateka ignimbrites. The Wharo Ignimbrite is the least evolved of these four ignimbrites but lies along the mixing line of the two magma compositions identified in the Welcome Bay and Arateka ignimbrites, and hence may represent a (relatively) mafic end-member from this system. The glass analyses of Otawera Ignimbrite are distinct from those of the other three ignimbrites: it has lower Al_2O_3, CaO, and Sr, and high abundances of Na_2O, K_2O, Rb, Ba, Y and higher Ba/Sr and Rb/Sr trace-element ratios.

Table 3. Summary of proximal ignimbrites and distal tephra correlatives and sources proposed in this study for the Tauranga ignimbrites and Hawke's Bay tephra deposits.

Unit names (this study)			**Correlatives**	
Proximal	***Distal***	***Source****	***Onshore***	***Offshore***
	Te Puna Ignimbrite	MVC	Kidnappers Ignimbrite; OH-16-01[1,2]	-
Waitеariki Ignimbrite	Hikuroa Pumice Member	TgaVC	KATY824 (?)[3]	M2[4]
Otawera Ignimbrite	-	TgaVC	-	-
Arateka Ignimbrite[5]	Esk Mst-T1	TgaVC	RIS-16-04[2]	M4[4]
-	-	TgaVC (?)	Ris-16-03[2]	M5
-	-	TgaVC (?)	Ris-16-01[2]	M6
-	Esk Mst-T2	TgaVC	OH-16-03; RIS-16-02; Ohingaiti 1[6]	M7[4]
Wharo Ignimbrite[7]	-	TgaVC	-	-
Welcome Bay Ignimbrite[7]	-	TgaVC	SA470 (?)[3]	-

*MCV, Mangakino Volcanic Centre; TgaVC, Tauranga Volcanic Centre

[1]Cooper *et al.* (2012)
[2]Hopkins and Seward (2019)
[3](?) = probable correlation, Milicich *et al.* (2013b)
[4]Stevens (2010)
[5]Previously known as Upper Pāpāmoa Ignimbrite (Briggs *et al.*, 2005)
[6]Naish *et al.* (1996)
[7]Previously known as Lower Pāpāmoa Ignimbrite (Briggs *et al.*, 2005)

Glass analyses of the Esk-Mudstone tephras T1 and T2 are compared with those of the four proximal TgaVC ignimbrites (Arateka, Welcome Bay, Wharo, and Otawera) in **Fig. 9**. The analyses of the Esk-Mst-T1 tephra show bimodal populations overlapping with those for the Arateka and Welcome Bay ignimbrites. Since the Welcome Bay Ignimbrite is older than either Esk Mst-T1 or -T2, it is likely therefore that Esk-Mst-T1 and the Arateka Ignimbrite represent the same eruptive event (**Table 3**). In contrast, the glass composition of Esk-Mst-T2 excludes any correlation to the proximal Pāpāmoa ignimbrites (Arateka, Welcome Bay, Wharo, and Otawera) analysed in this study. However, an undefined source within the TgaVC remains likely because of the broad similarities in age.

Hopkins and Seward (2019) identified a sequence of five tephras within a mudstone at Rissington and within the Ohara Depression in Hawke's Bay **(Fig. 2b)**. Their tephras OH-16-03 and RIS-16-02 were identified as correlatives, providing a tie point between the sequences at the two locations. Kamp *et al.* (2007) identified deposits at these locations as part of the Esk Mudstone Formation, and so we have compared the glass compositions of tephras RIS-16-01 to RIS-16-04, and OH-16-03 (of Hopkins and Seward, 2019), with those of Esk-Mst-T1 and T2 to see if any are correlatives **(Fig. 9)**. Glass analyses of Esk-Mst-T2 and RIS-16-02/OH-16-03 are essentially identical with regard to both major and trace elements and, along with stratigraphic positioning, meaning that these deposits are very likely to be correlatives.

Although strong similarities within the glass major elements are evident for Esk-Mst-T1 and RIS-16-01, RIS-16-03, and RIS-16-04, these units can be distinguished as separate eruptive deposits on the basis of glass trace-element abundances and ratios **(Fig. 9)**. RIS-16-04 glass has a composition which strongly represents that of the high-SiO_2 population of Esk-Mst T1/Arateka Ignimbrite, and both these tephra-fall units represent the youngest deposit in each respective location, with RIS-16-01 and RIS-16-03 stratigraphically older, but above RIS-16-02/OH-16-03/Esk Mst-T2 **(Table 3).** Strong chemical similarities are also evident in glass analyses from offshore deposits ODP 1124C 7H-4 (M4-1 and M4-2) and ODP 1124C 7H-6 (M7) (Stevens, 2010). The glass composition of tephra M7 consistently overlaps with that of Esk Mst-T2, and RIS-16-02/OH-16-03 and M4 show the same two chemical populations found within Esk Mst-T1. In addition, the stratigraphic relationships of the tephras are consistent both onshore and offshore, and hence the deposits can be identified as correlatives **(Table 3)**. Therefore, it is likely that the middle two tephras in the Rissington sequence of Hopkins and Seward (2019), RIS-16-01 and RIS-16-03, either were not deposited or were not preserved in the Waikoau River area **(Fig. 2b)**.

5.1.2 Waitearikí Ignimbrite and Hikuroa Pumice Member

The U-Pb zircon ages for the Waitearikí Ignimbrite provide an average maximum eruptive age of 2.1 Ma **(Table 1)**. This age is consistent with previous K-Ar age determinations of 2.18 ± 0.15 Ma (whole-rock) and 2.13 ± 0.17 Ma (plagioclase) (Takagi, 1995), an $^{40}Ar/^{39}Ar$ age of 2.09 ± 0.03 Ma (Briggs *et al.*, 2005) and a (U/Th)/He zircon age of 2.25 ± 0.26 Ma (Pittari *et al.*, 2021).

Milicich *et al.* (2013b) described two ignimbrites, KATY824 and SA470, found within drill cores from the Kawerau Geothermal Field **(Fig. 1)** and suggested that these deposits may be correlatives of the Waitearikí and Welcome Bay ignimbrites on the basis of similar U-Pb zircon ages of 2.17 ± 0.05 Ma (KATY824) and 2.38 ± 0.05 Ma (SA470), respectively. In addition to similar ages for the Waitearikí Ignimbrite, KATY824 and SA470 have mineral assemblages of plagioclase, quartz, altered ferromagnesian minerals, biotite, minor lithics of rhyolitic lava and, in KATY824, a eutaxitic texture (Milicich *et al.*, 2013a). These mineralogical characteristics are consistent with those of the Waitearikí and Welcome Bay ignimbrites, and hence (together with the age data) support a probable correlation between these deposits. Because of the intense alteration, comparison of glass composition between KATY824 and SA470, and that of TgaVC ignimbrites is not feasible.

The brown-coloured glass in the lower Waitearikí Ignimbrite was examined using a scanning electron microscope prior to analysis. This investigation demonstrated that microlite development from devitrificaton is not widespread at this stratigraphic level, although a degree of post-depositional hydration is a certainty due to the formation of perilitic cracking within the fiamme (Denton *et al.*,

2009). However, the relatively high analytical totals and consistent geochemical composition **(Table 2)** obtained in our study indicate that the brown Waiteariki glass remains a fair approximation of melt composition. Comparison of glass composition of the Hikuroa Pumice Member with that of Waiteariki Ignimbrite is shown in **Fig. 10.** The two ignimbrites have extremely similar major and trace element abundances and trace-element ratios, although **Figure 10a** shows a systematic offset in the FeO_t (-0.35 wt %) and CaO (+0.11 wt %), which may be linked to the 'browning' of the Waiteariki Ignimbrite glass. Based on major and trace element geochemistry, corresponding stratigraphic positions and ages, we conclude that the Waiteariki Ignimbrite and Hikuroa Pumice Member are correlatives.

Glass-analysis-derived bivariate plots of FeO_t vs CaO, and plots of trace-element ratios of large ion lithophile (LIL) elements (e.g. Ba and Rb vs Sr) against Zr/Y **(Fig. 10a and b)**, show a bimodal composition for the Hikuroa Pumice Member where lower FeO_t, CaO and Zr/Y ratios along with higher LIL ratios, define a distinct sub-group **(e.g. Fig. 10f)**. This sub-group, however, is not observed in the equivalent glass analyses from the proximal Waiteariki ignimbrite which may reflect the limited stratigraphic interval sampled because of the predominance of unsuitable glass, or geochemical zonation within the proximal deposit. Glass from deposits at the three distal sites (Darkys Spur, Beattie Road and McIntyre Access Road) show this sub-group but no link with stratigraphic position within the deposit nor SiO_2 content can be discerned. Therefore, it remains unclear if this bimodality reflects the eruption of a magma source with systematic zonation with subsequent mixing of shards during transportation of > 150 km from the source region, tapping of discrete magma batches, or both.

Previous studies have correlated the Hikuroa Pumice Member to the offshore deposit ODP 1124C 7H 3W (M2) (Bland *et al.*, 2007; Stevens, 2010; Hopkins & Seward, 2019). Hopkins and Seward (2019) investigated a potential link between the Hikuroa Pumice Member and known tephra deposits of similar age in the Whanganui Basin **(Fig. 1)**, but no correlatives have yet been identified.

5.1.3 Te Puna Ignimbrite

This study dates the Te Puna Ignimbrite at 1.11 ± 0.046 Ma, a little older than the previously determined $^{40}Ar/^{39}Ar$ age of 0.929 ± 0.012 Ma (Briggs *et al.*, 2005). The Rocky Hill and Kidnappers ignimbrites were erupted from the MVC around this time, the former being separated from the Kidnappers Ignimbrite by an erosional surface which represents a period of only years to decades (possibly ~10–20 years) (Cooper *et al.*, 2017). The two ignimbrites share the same magmatic system, and the very close time span between the two eruptions means the eruptive glasses have extremely similar major and trace element compositions **(Fig. 11)**. The Rocky Hill Ignimbrite, however, was a much smaller eruption volumetrically (although still substantial, c. 200 km^3 DRE) with deposits restricted to the west and north of the Mangakino Caldera **(Fig. 1)**. Juvenile clasts have a distinct

texture which includes large (up to 5 mm), euhedral amphibole crystals and only minor biotite which allows the unit to be distinguished from Kidnappers Ignimbrite. Three geochemical populations have been identified within the Kidnappers ignimbrite, with Groups 1 and 2 being more volumetrically significant (Cooper *et al.* 2012). **Fig. 11** demonstrates that the glass composition of the Te Puna Ignimbrite is highly consistent with that of the Kidnappers Ignimbrite and contains shards of both Group 1 and 2 glass compositions. The offset in SiO_2 in **Fig. 11c** is likely to be an artefact of data normalization, where SiO_2 values can vary upwards of 5 wt % when analytical totals are low (e.g. 91.7–99%, average 95.86 %: Cooper *et al.* 2016); 98.45-99.44 %, average 98.97%, our study). Despite this, SiO_2 averages for Kidnappers Group 1 and Te Puna glass still overlap within error. Bivariate plots of trace-element and trace-element-ratio data **(Fig. 11d-f)** also show consistent overlap in geochemical composition and augment the correlation suggested from the major element glass compositions.

Our new data (equivalent age, identical glass composition, mineralogy, similar textures) suggest that the Te Puna and Kidnappers ignimbrites are correlatives. However, Briggs *et al.* (2005) refers to unpublished paleomagnetic data which states the Te Puna Ignimbrite is reversely magnetised. This orientation, however, conflicts with a normal polarity (Jaramillo subchron) reported for the Kidnappers Ignimbrite (Cooper *et al.*, 2012), which would exclude such a correlation. Notwithstanding, we propose that based on the numerous lines of evidence presented here, the Te Puna Ignimbrite is highly likely to be a correlative of the Kidnappers Ignimbrite. The magnetic polarity of these units should be re-examined to authenticate the unpublished palaeomagnetic data before the correlation proposed here can be excluded.

5.2. Implications of correlations

We have correlated a number of the TgaVC-derived proximal ignimbrite deposits of the Tauranga region, and the MVC-derived Te Puna Ignimbrite, with deposits in northern Hawke's Bay and elsewhere as summarised in **Table 3**. These correlations show that deposits from explosive rhyolitic volcanism of the TgaVC are more extensive than previously recognised.

Five separate ignimbrite-forming eruptions are currently recognised as occurring in the TgaVC, namely Arateka, Welcome Bay, Wharo, Otawera ignimbrites (previously undifferentiated deposits of the Pāpāmoa Formation of Briggs *et al.*, 1996, 2005), and the Waitearikiignimbrite. These five eruptives are likely a minimum because our knowledge of the proximal stratigraphy of the Pāpāmoa Range remains incomplete. Local investigations are hampered by limited outcrop exposures due to subsequent burial by younger TVZ-derived deposits and pervasive devitrification and/or welding of deposits. Additionally, the sample of Upper Pāpāmoa Ignimbrite dated by Briggs *et al.*, (2005) was not

collected from the type locality for this unit. Instead, it appears to be a sample derived from an unrecognised ignimbrite that was erupted after the Waitieariki Ignimbrite.

The identification of distal deposits of the Waitieariki Ignimbrite located throughout northern Hawke's Bay suggests the eruption of the Waitieariki Ignimbrite was a significant large-scale silicic event. Large-volume silicic eruptions have been common throughout the history of the TVZ with 25 inferred caldera-forming eruptions taking place in the last 1.6 Ma ranging in volume from 30 to 1500 km^3 (Wilson *et al.*, 2009). The largest four eruptions are classed as supereruptions, and include the Ongatiti (>500 km^3 DRE; Yousef, 2020) and Kidnappers ignimbrites (1200 km^3 DRE; Cooper *et al*., 2012) from the Mangakino Volcanic Centre, the Whakamaru-group ignimbrites (2200 km^3 DRE; Gravely *et al.*, 2016), Whakamaru caldera and the Oruanui Ignimbrite (>530 km^3 DRE; Barker *et al.*, 2021) from the Taupō caldera. While the runout distances of ignimbrites can vary considerably, such distances are directly related to increasing mass flow rates feeding the pyroclastic currents and bulk volumes (Giordano and Cas, 2021). Of the New Zealand supereruptions, the runouts vary from c. 75 km for the Whakamaru ignimbrites, to 90, 140 and 180 km for the Oruanui, Ongatiti, and Kidnappers ignimbrites, respectively (Wilson *et al.*, 1995; Alloway *et al.*, 2004; Barker *et al.*, 2021). The runout distance for the Waitieariki Ignimbrite is ambiguous as the eruptive source is still to be determined precisely. However, it is assumed to be within the TgaVC (Briggs *et al.*, 2005) and so the location of distal deposits ~150 km south-east of TgaVC, implies that the Waitieariki Ignimbrite is almost certainly the product of a caldera-forming eruption and has the potential to be one of the largest eruptive events in New Zealand's geological record. The caldera source of the Waitieariki, and possibly other ignimbrites within the TgaVC is yet to be formally defined (Prentice *et al.*, 2020; Pittari *et al.*, 2021) and the link between these and the numerous rhyolite domes found throughout the region is yet to be investigated, but both would likely share a common magmatic system with any local caldera.

The Esk Mudstone tephra-T1, a correlative of Rissington RIS-16-04 (Hopkins & Seward, 2019), was able to be positively matched to the proximal Arateka Ignimbrite. The new U-Pb zircon ages for the Esk Mudstone tephras T1 and T2 provide the first radiometric age constraints for the lower Esk Mudstone Formation of c. 2.2 Ma and significantly extends the known extent of these tephra-fall deposits. The ages on the Esk Mudstone tephras, together with those of the five TgaVC-derived ignimbrites, and other deposits of the TgaVC (Briggs *et al.*, 2005; Pittari *et al.*, 2021), indicate that the period from c. 2.4 to 2.0 Ma was a period of frequent rhyolitic activity in northern New Zealand, which culminated with the eruption of the large-volume Waitieariki Ignimbrite. From the combined proximal and distal records, we identify eight rhyolitic events over this period, giving an average repose period for the TgaVC of c. 50 kyrs. We stress that this is a maximum value as local dome eruptions have been excluded due to uncertain links between them and known tephra deposits. As previously noted, it is

also likely that there are further ignimbrites to be defined in the southern Pāpāmoa Range. In comparison, a repose period for late CVZ activity (c. 7–3.5 Ma) was determined to be c. 75 kyrs (Stevens, 2010). It is worth noting, that older records, such as those for the TgaVC and CVZ, are likely to be biased towards larger (more voluminous) events that would tend to have greater preservation potential in both proximal and distal locations. The TVZ is known to be one of the most prolific silicic eruption centres on Earth, with voluminous ignimbrites occurring every c. 50 kyrs over the past 1.6 Myrs (Wilson *et al.*, 2005; Gravley *et al.*, 2016). However, this average repose period disguises several clusters of activity which occurred at 1.2, 1.0, 0.35, and 0.06 Ma, referred to as short ignimbrite flare-up events (Gravley *et al.*, 2016). The largest of these flare-up events occurred from ~350 to ~280 ka, where at least eight large ignimbrite eruptions occurred in <100 kyrs. The frequency of silicic volcanism from the TgaVC is similar to that of the TVZ, with voluminous ignimbrite eruptions occurring on average every 50 kyrs, but, as with the TVZ, many of these events occurred clustered in time. For example, the four ignimbrite eruptions in TgaVC of Welcome Bay, Wharo, Otawera, and Arateka ignimbrites, occurred within c. 90 kyrs between 2.3 and 2.2 Ma, and therefore may represent an early ignimbrite flare-up event, similar to those described for the TVZ.

Borehole geological data from TVZ geothermal wells implies continuing rhyolitic volcanism between c. 2 and 1.6 Ma (Chambefort *et al.*, 2014; Milicich *et al.*, 2020). This period covers suspected caldera volcanism of late TgaVC activity and the onset of volcanism at MVC, but it is not known whether these deposits are related in any way to volcanism originating from either centre, or an additional unrecognised silicic system (or caldera) with an overlapping eruptive timespan, a phenomenon well recognised within young and modern TVZ periods (Charlier *et al.*, 2003; Gravley *et al*., 2007, 2016). Originating from the Mangakino Caldera, the Kidnappers Ignimbrite is exceptionally widespread ignimbrite with a known distribution stretching from Auckland to Hawke's Bay (Wilson *et al.*, 1995; Cooper *et al.*, 2012). The confirmed correlation between the Te Puna and Kidnappers ignimbrites formally extends the known distribution of this eruptive into the Tauranga region.

7. Conclusions

The Tauranga Volcanic Centre (TgaVC), active from 2.95 to 1.9 Ma, lies temporally and spatially between the defined locations and time frames of activity in the CVZ and the currently active TVZ, one of the most productive regions of Quaternary silicic volcanism on Earth. New U-Pb zircon ages and major and trace element glass compositional analyses of five prominent proximal ignimbrites from the TgaVC confirm previously postulated links between these units and age-equivalent tephra deposits in northern Hawke's Bay. The Arateka ignimbrite (correlative Esk Mst-T1) and Esk Mst-T2 tephra provide the first radiometric age constraints (2.2 Ma) for the lower Esk Mudstone Formation, and a robust

isochronous tie point for the wider region. The Hikuroa Pumice Member in Hawke's Bay is a distal ignimbrite found 150-170 km southeast from the southern-most exposures of its proximal (coeval) equivalent, the Waiteariki Ignimbrite. Hence these eruptive products are distributed more extensively than previously recognised. Volcanic activity in the TgaVC documented here, and the record of tephra deposits elsewhere, indicates that rhyolitic activity in New Zealand between 2.4 and 2 Ma was frequent: at least eight eruptions occurred within TgaVC, culminating with the eruption of the very large-volume Waiteariki Ignimbrite at 2.1 Ma. This record provides a maximum mean repose period for the TgaVC of ca. 50 kyrs. Our study demonstrates the importance of combining proximal and distal records in reconstructing the early eruptive histories of active volcanic regions, and the newly-established correlation between the Hikuroa Pumice Member and Waiteariki Ignimbrite will form the basis for further investigations to define the distribution, volume and source caldera for the Waiteariki Ignimbrite. Our findings also allow the transition of volcanic activity from the previously active CVZ to the TVZ to be reassessed and have implications for our understanding of the onset of large-volume rhyolitic activity during the Early Quaternary at the dawn of the TVZ.

Acknowledgments

This research was funded by a University of Waikato Doctoral Scholarship and a School of Science Trust Fund Research Grant. MLP thanks Jenni Hopkins for discussions on the tephrostratigraphy of Hawke's Bay and Whanganui Basins; Matt Sagar for advice on common Pb corrections and calculation of U-Pb ages; and field and laboratory assistance from Rochelle Hansen, Edie Fisher, Kirsty Vincent and Annette Rodgers. We would also like to thank two anonymous reviewers for helpful comments that helped clarify and improve this manuscript and Jose Luis Macias for editorial handling. This paper is an output of the Commission on Tephrochronology (COT) of the International Association of Volcanism and Chemistry of the Earth's Interior (IAVCEI).

References

Amma-Miyasaka, M., Miura, D., Nakagawa, M., Uesawa, S., & Furukawa, R. (2020). Stratigraphy and chronology of silicic tephras in the Shikotsu-Toya volcanic field, Japan: Evidence of a Late Pleistocene ignimbrite flare-up in southwestern Hokkaido. *Quaternary International, 562*, 58-75.

Bland, K. J., Kamp, P. J., & Nelson, C. S. (2007). *Systematic lithostratigraphy of the Neogene succession exposed in central parts of Hawke's Bay Basin, eastern North Island, New Zealand*. Hamilton, New Zealand: The University of Waikato.

Briggs, R., Houghton, B., McWilliams, M., & Wilson, C. (2005). 40Ar/39Ar ages of silicic volcanic rocks in the Tauranga-Kaimai area, New Zealand: Dating the transition between volcanism in the Coromandel Arc and the Taupo Volcanic Zone. *New Zealand Journal of Geology and Geophysics, 48*(3), 459-469.

Briggs, R. M., Hall, G. J., Harmsworth, G. R., Hollis, A. G., Houghton, B. F., Hughes, G. R., Morgan, M. D., & Whitbread-Edwards, A. R. (1996). *Geology of the Tauranga area: sheet U14 1:50 000*. Hamilton, N.Z.: Hamilton, N.Z. : Dept. of Earth Sciences, University of Waikato.

Bryant, C., Arculus, R., & Eggins, S. (2003). The geochemical evolution of the Izu-Bonin arc system: A perspective from tephras recovered by deep - sea drilling. *Geochemistry, Geophysics, Geosystems, 4*(11).

Carter, L., Alloway, B., Shane, P., & Westgate, J. (2004). Deep-ocean record of major late Cenozoic rhyolitic eruptions from New Zealand. *New Zealand Journal of Geology and Geophysics, 47*(3), 481-500.

Chambefort, I., Lewis, B., Wilson, C., Rae, A., Coutts, C., Bignall, G., & Ireland, T. (2014). Stratigraphy and structure of the Ngatamariki geothermal system from new zircon U–Pb geochronology: Implications for Taupo Volcanic Zone evolution. *Journal of Volcanology and Geothermal Research, 274*, 51-70.

Charlier, B. L. A., Peate, D. W., Wilson, C. J. N., Lowenstern, J. B., Storey, M., & Brown, S. J. A. (2003). Crystallisation ages in coeval silicic magma bodies: 238U–230Th disequilibrium evidence from the Rotoiti and Earthquake Flat eruption deposits, Taupo Volcanic Zone, New Zealand. *Earth and Planetary Science Letters, 206*(3), 441-457.

Cheng, H., Edwards, R. L., Shen, C.-C., Polyak, V. J., Asmerom, Y., Woodhead, J., Hellstrom, J., Wang, Y., Kong, X., & Spötl, C. (2013). Improvements in 230Th dating, 230Th and 234U half-life values, and U–Th isotopic measurements by multi-collector inductively coupled plasma mass spectrometry. *Earth and Planetary Science Letters, 371*, 82-91.

Cooper, G. F., Morgan, D. J., & Wilson, C. J. (2017). Rapid assembly and rejuvenation of a large silicic magmatic system: Insights from mineral diffusive profiles in the Kidnappers and Rocky Hill deposits, New Zealand. *Earth and Planetary Science Letters, 473*, 1-13.

Cooper, G. F., Wilson, C. J., Millet, M.-A., & Baker, J. A. (2016). Generation and rejuvenation of a supervolcanic magmatic system: a case study from Mangakino volcanic centre, New Zealand. *Journal of Petrology, 57*(6), 1135-1170.

Cooper, G. F., Wilson, C. J., Millet, M.-A., Baker, J. A., & Smith, E. G. (2012). Systematic tapping of independent magma chambers during the 1 Ma Kidnappers supereruption. *Earth and Planetary Science Letters, 313*, 23-33.

Cunningham, M. J., Lowe, D. J., Wyatt, J. B., Moon, V. G., & Churchman, G. J. (2016). Discovery of halloysite books in altered silicic Quaternary tephras, northern New Zealand. *Clay Minerals, 51*(3), 351-372.

Downs, D., Rowland, J., Wilson, C., Rosenberg, M., Leonard, G., & Calvert, A. (2014). Evolution of the intra-arc Taupo-Reporoa Basin within the Taupo Volcanic Zone of New Zealand. *Geosphere, 10*(1), 185-206.

Gravley, D., Deering, C., Leonard, G., & Rowland, J. (2016). Ignimbrite flare-ups and their drivers: A New Zealand perspective. *Earth-Science Reviews, 162*, 65-82.

Gravley, D. M., Wilson, C. J. N., Leonard, G. S., & Cole, J. W. (2007). Double trouble: Paired ignimbrite eruptions and collateral subsidence in the Taupo Volcanic Zone, New Zealand. *GSA Bulletin, 119*(1-2), 18-30.

Healy, J. (1967). Geological report on proposed tunnel line, Kaimai Railway Deviation. *NZ Geological Survey, DSIR, unpublished report file T14/90-99: 68p*.

Hegan, B. D. (1972). *Kaimai railway deviation. Kaimai Tunnel, eastern side geological investigations.* NZ Geological Survey, DSIR, unpublished report file EG 129: 3p.

Hopkins, J. L., Lowe, D. J., & Horrocks, J. L. (2021a). Tephrochronology in Aotearoa New Zealand. *New Zealand Journal of Geology and Geophysics, 64(1-2)*, 153-200.

Hopkins, J. L., Bidmead, J. E., Lowe, D. J., Wysoczanski, R. J., Pillans, B. J., Ashworth, L., Rees, A. B., & Tuckett, F. (2021b). TephraNZ: a major- and trace-element reference dataset for glass-shard analyses from prominent Quaternary rhyolitic tephras in New Zealand and implications for correlation. *Geochronology, 3(2)*, 465-504.

Hopkins, J. L., & Seward, D. (2019). Towards robust tephra correlations in early and pre-Quaternary sediments: A case study from North Island, New Zealand. *Quaternary Geochronology, 50*, 91-108.

Houghton, B. F., & Cuthbertson, A. S. (1989). *Kaimai sheet T14 BD*. Lower Hutt, Wellington, N.Z.: New Zealand Geological Survey, Department of Scientific and Industrial Research.

Kamp, P. J., Bland, K. J., Caron, V., Graafhuis, R. B., Baggs, R. A., Dyer, S. D., Boyle, S. F., & Nelson, C. S. (2007). *Stratigraphic columns for the Neogene succession exposed in central parts of Hawke's Bay Basin, eastern North Island, New Zealand*. Hamilton, New Zealand: The University of Waikato.

Kilgour, G., & Smith, R. (2008). Stratigraphy, dynamics, and eruption impacts of the dual magma Rotorua eruptive episode, Okataina Volcanic Centre, New Zealand. *New Zealand Journal of Geology and Geophysics, 51*(4), 367-378.

Kutterolf, S., Schindlbeck, J., Anselmetti, F. S., Ariztegui, D., Brenner, M., Curtis, J., Schmid, D., Hodell, D., Mueller, A., & Pérez, L. (2016). A 400-ka tephrochronological framework for Central America from Lake Petén Itzá (Guatemala) sediments. *Quaternary Science Reviews, 150*, 200-220.

Le Maitre, R. W., Streckeisen, A., Zanettin, B., Le Bas, M., Bonin, B., & Bateman, P. (2002). *Igneous rocks: a classification and glossary of terms: recommendations of the International Union of Geological Sciences Subcommission on the Systematics of Igneous Rocks*. Cambridge University Press.

Leonard, G. S., Begg, J. G., & Wilson, C. J. N. (2010). *Geology of the Rotorua area. Institute of Geological & Nuclear Sciences 1:250 000 geological map5*. 1 sheet + 102p. Lower Hutt, New Zealand. GNS Science.

Lowe, D. J. (2011). Tephrochronology and its application: A review. *Quaternary Geochronology, 6*(2), 107-153.

Lowe, D. J., Pearce, N. J., Jorgensen, M. A., Kuehn, S. C., Tryon, C. A., & Hayward, C. L. (2017). Correlating tephras and cryptotephras using glass compositional analyses and numerical and statistical methods: Review and evaluation. *Quaternary Science Reviews, 175*, 1-44.

Lukács, R., Harangi, S., Guillong, M., Bachmann, O., Fodor, L., Buret, Y., Dunkl, I., Sliwinski, J., von Quadt, A., & Peytcheva, I. (2018). Early to Mid-Miocene syn-extensional massive silicic volcanism in the Pannonian Basin (East-Central Europe): eruption chronology, correlation potential and geodynamic implications. *Earth-science reviews, 179*, 1-19.

Milicich, S., Chambefort, I., Wilson, C., Alcaraz, S., Ireland, T., Bardsley, C., & Simpson, M. (2020). A zircon U-Pb geochronology for the Rotokawa geothermal system, New Zealand, with implications for Taupō Volcanic Zone evolution. *Journal of Volcanology and Geothermal Research, 389*, 106729.

Milicich, S. D., Wilson, C. J. N., Bignall, G., Pezaro, B., & Bardsley, C. (2013a). Reconstructing the geological and structural history of an active geothermal field: A case study from New Zealand. *Journal of Volcanology and Geothermal Research, 262*, 7-24.

Milicich, S. D., Wilson, C. J. N., Bignall, G., Pezaro, B., Charlier, B. L. A., Wooden, J. L., & Ireland, T. R. (2013b). U–Pb dating of zircon in hydrothermally altered rocks of the Kawerau Geothermal Field, Taupo Volcanic Zone, New Zealand. *Journal of Volcanology and Geothermal Research, 253*, 97-113.

Naish, T., Kamp, P. J., Alloway, B. V., Pillans, B., Wilson, G. S., & Westgate, J. A. (1996). Integrated tephrochronology and magnetostratigraphy for cyclothemic marine strata, Wanganui Basin: implications for the Pliocene-Pleistocene boundary in New Zealand. *Quaternary International, 34*, 29-48.

Namaliu, M. (2021). *Volcanic geology of the early Pleistocene ignimbrite succession in the western Papamoa Region, Bay of Plenty (MSc thesis).* University of Waikato, Hamilton, New Zealand.

Paton, C., Hellstrom, J., Paul, B., Woodhead, J., & Hergt, J. (2011). Iolite: Freeware for the visualisation and processing of mass spectrometric data. *Journal of Analytical Atomic Spectrometry, 26*(12), 2508-2518.

Pearce, N. J., Westgate, J. A., Gualda, G. A., Gatti, E., & Muhammad, R. F. (2020). Tephra glass chemistry provides storage and discharge details of five magma reservoirs which fed the 75 ka Youngest Toba Tuff eruption, northern Sumatra. *Journal of Quaternary Science, 35*(1-2), 256-271.

Pearce, N. J. G., Perkins, W. T., Westgate, J. A., & Wade, S. C. (2011). Trace-element microanalysis by LA-ICP-MS: the quest for comprehensive chemical characterisation of single, sub-10 µm volcanic glass shards. *Quaternary International, 246*(1-2), 57-81.

Petrus, J. A., & Kamber, B. S. (2012). VizualAge: A novel approach to laser ablation ICP‐MS U‐Pb geochronology data reduction. *Geostandards and Geoanalytical Research, 36*(3), 247-270.

Pittari, A., Prentice, M. L., McLeod, O. E., Yousef Zadeh, E., Vincent, K. A., Kamp, P. J. J., & Danisik, M. (2021). Inception of the modern North Island (New Zealand) volcanic setting: Spatio-temporal patterns of volcanism between 3.0 and 0.9 Ma. *New Zealand Journal of Geology and Geophysics, 64(1-2)*, 250-272.

Ponomareva, V., Bubenshchikova, N., Portnyagin, M., Zelenin, E., Derkachev, A., Gorbarenko, S., Garbe-Schönberg, D., & Bindeman, I. (2018). Large-magnitude Pauzhetka caldera-forming eruption in Kamchatka: Astrochronologic age, composition and tephra dispersal. *Journal of Volcanology and Geothermal Research, 366*, 1-12.

Ponomareva, V., Portnyagin, M., & Davies, S. M. (2015). Tephra without borders: far-reaching clues into past explosive eruptions. *Frontiers in Earth Science, 3*, 83.

Prentice, M. L., Pittari, A. K., P., Lowe, D. J., & Kilgour, G. (2020). The 2.1 Ma Waitearíki Ignimbrite: defining a new supereruption at the onset of TVZ volcanism. In K. N. Bassett*, et al.* (Eds.), *Geosciences 2020: Abstract Volume. Geoscience Society of New Zealand Miscellaneous Publication 157A* (pp. 227). Wellington: Geoscience Society of New Zealand.

Sagar, M. W., Browne, G. H., Arnot, M. J., Seward, D., & Strogen, D. P. (2019). New U–Pb zircon ages and a revised integrated age model for the late Miocene northern Taranaki coastal section, New Zealand. *New Zealand Journal of Geology and Geophysics, 62*(3), 357-370.

Schärer, U. (1984). The effect of initial230Th disequilibrium on young UPb ages: the Makalu case, Himalaya. *Earth and Planetary Science Letters, 67*(2), 191-204.

Schneider, J.-L., Le Ruyet, A., Chanier, F., Buret, C., Ferrière, J., Proust, J.-N., & Rosseel, J.-B. (2001). Primary or secondary distal volcaniclastic turbidites: how to make the distinction? An example from the Miocene of New Zealand (Mahia Peninsula, North Island). *Sedimentary Geology, 145*(1-2), 1-22.

Silleni, A., Giordano, G., Isaia, R., & Ort, M. H. (2021). The Magnitude of the 39.8 ka Campanian Ignimbrite Eruption, Italy: Method, Uncertainties and Errors. *Frontiers in Earth Science*, 8, 444.Spencer, C. J., Kirkland, C. L., & Taylor, R. J. (2016). Strategies towards statistically robust interpretations of in situ U–Pb zircon geochronology. *Geoscience Frontiers, 7*(4), 581-589.

Stacey, J. S., & Kramers, J. D. (1975). Approximation of terrestrial lead isotope evolution by a two-stage model. *Earth and Planetary Science Letters, 26*(2), 207-221.

Steiger, R. H., & Jäger, E. (1977). Subcommission on geochronology: convention on the use of decay constants in geo-and cosmochronology. *Earth and planetary science letters, 36*(3), 359-362.

Stevens, M. T. (2010). Miocene and Pliocene Silicic Coromandel Volcanic Zone Tephras from ODP Site 1124-C: Petrogenetic Applications and Temporal Evolution.

Stipp, J. J. (1968). *The geochronology and petrogenesis of the Cenozoic volcanics of North Island, New Zealand (PhD thesis)*. Canberra, Australia: Australian National University.

Straub, S. M., Woodhead, J. D., & Arculus, R. J. (2015). Temporal evolution of the Mariana Arc: Mantle wedge and subducted slab controls revealed with a tephra perspective. *Journal of Petrology, 56*(2), 409-439.

Sutton, A. N., Blake, S., Wilson, C. J., & Charlier, B. L. (2000). Late Quaternary evolution of a hyperactive rhyolite magmatic system: Taupo volcanic centre, New Zealand. *Journal of the Geological Society, 157*(3), 537-552.

Takagi, M. (1995). *Miocene-Pliocene arc volcanism of the Hauraki region in North Island, New Zealand (MSc thesis)*. Okayama, Japan: Hiruzen Research Institute.

Vermeesch, P. (2018). IsoplotR: A free and open toolbox for geochronology. *Geoscience Frontiers, 9*(5), 1479-1493.

White, J., & Houghton, B. (2006). Primary volcaniclastic rocks. *Geology, 34*(8), 677-680.

Williams, I. S. (1998). U-Th-Pb geochronology by ion microprobe. *Reviews in economic geology, 7*, 1-35.

Wilson, C., Houghton, B., Kampt, P., & McWilliamst, M. (1995). An exceptionally widespread ignimbrite with implications for pyroclastic flow emplacement. *Nature, 378*(6557), 605-607.

Wilson, C. J. N., & Rowland, J. V. (2016). The volcanic, magmatic and tectonic setting of the Taupo Volcanic Zone, New Zealand, reviewed from a geothermal perspective. *Geothermics, 59, Part B*, 168-187.